Date of Publish: 25/05/2018

Linear Motor Compressor Controller Design Report

Designed by:

Electrical and Electronic Design Limited

Commissioned by:

Fisher & Paykel New Zealand Limited

Written by:

Abin Thomas,

Arun Ravindran,

Hasnain Cheena

& James Shore

Fisher&Paykel

Abstract

This report has been commissioned by Fisher & Paykel Appliances New Zealand (FPA) to describe the design of a controller for the linear compressor found in Fisher & Paykel fridges. FPA aims to use this controller in multiple fridge models, which they target at premium appliance customers. The purpose of this report is to outline the viability of a design that was implemented as a prototype and tested under laboratory conditions, using a simplified model of a linear compressor. Findings from simulation and testing indicated that the product will be a feasible and effective addition to fridges produced by FPA. Its associated cost is in the area of $7.60 NZD per unit. The report will outline design decisions, constraints, costing, and feasibility considerations.

Table of Contents

Abstract 2
Table of Contents 3
Table of Figures 4
Table of Tables 5
Introduction 6
1.0 Design Functionality 8
1.1 Overview 8
1.2 Internal Power Supply 8
1.3 H-Bridge 9
1.4 Voltage Sensing 10
1.5 Current Sensing 10
1.6 Communications Circuit 11
2.0 Code Functionality 13
2.1 Software Architecture Diagram 13
2.2 Main Loop 14
2.3 UART Receive ISR 14
2.4 UART Transmit ISR 15
2.5 Pulse-Width Modulation ISR 15
3.0 Cost of Design 16
4.0 Manufacturing Considerations 17
5.0 Testing Overview 18
6.0 Design Feasibility 20
7.0 Conclusions 21
8.0 References 22
Appendix A: Implementation Details 23
Appendix A1: Selection of Main Components 25
Appendix A2: Derivation of Design Equations 25
Appendix A3: Choosing Component Values 34
Appendix A4: Code Functionality Details 41
Appendix B: Costing Particulars 43
Appendix B1: Materials Cost 44
Appendix B2: Running Costs 45
Appendix C: Bill of Materials 47
Appendix D: Testing 48
Appendix D1: Regression Analysis 48

Appendix D2: Hardware Testing Results 49
Appendix E: Developmental Process 53
Appendix F: Manufacturing Considerations 55
Appendix G: Technical Specifications 56

Table of Figures

Figure 1: Overall Functional Block Diagram ..... **Error! Bookmark not defined.**
Figure 2: Integrated Circuit 5V Regulator Block Diagram ..... **Error! Bookmark not defined.**
Figure 3: H-Bridge Block Diagram ..... **Error! Bookmark not defined.**
Figure 4: Voltage Sensing Block Diagram ..... **Error! Bookmark not defined.**
Figure 5: Current Sensing Block Diagram ..... **Error! Bookmark not defined.**
Figure 6: Communication Circuit Block Diagram ..... **Error! Bookmark not defined.**
Figure 7: Overall Code Flowchart ..... **Error! Bookmark not defined.**
Figure 8: Main Loop Flowchart ..... **Error! Bookmark not defined.**
Figure 9: UART Receive Flowchart ..... **Error! Bookmark not defined.**
Figure 10: UART Transmit Flowchart ..... **Error! Bookmark not defined.**
Figure 11: PWM Flowchart ..... **Error! Bookmark not defined.**
Figure 12: Picture of Linear Motor Rig ..... **Error! Bookmark not defined.**
Figure 13: Flow Rate vs MFC Request Graph ..... **Error! Bookmark not defined.**
Figure A1: Schematic of the H-bridge 23
Figure A2: Schematic of the Supplies 23
Figure A3: Schematic of the communication circuit 23
Figure A4: Schematic of the Current Sensing 24
Figure A5: Schematic of Voltage Sensing 24
Figure A6: Schematic of Microcontroller 24
Figure A2.1: Schematic of PMOS Gate Driver ..... **Error! Bookmark not defined.**
Figure A2.2: Schematic of Current Sense Low Pass Filter ..... **Error! Bookmark not defined.**
Figure A2.3: Schematic of Level Shifter and Amplifier 32
Figure A3.1: PMOS Gate Driver Circuit 35
Figure A3.2: Low Pass Filter Circuit 36
Figure A3.3: Level shift and gain amplifier circuit 38
Figure D1.1: Relationships between different variables 48
Figure D2.1: Waveform of NMOS Gate Voltage 49
Figure D2.2: Waveform of PMOS Gate Driver Input 50
Figure D2.3: Waveform of PMOS Gate Voltage 50
Figure D2.4: Waveform of Current Sense 51

Figure D2.5: Waveform of high-side voltage, when driving with one pair of MOSFETs 51
Figure D2.6: Waveform of low-side voltage, when driving with one pair of MOSFETs 52
Figure E1: Breadboard during development 54
Figure E2: Implementation on a PCB 54

Table of Tables

Table 1: Table showing the MFC Request vs Flow Rate 19
Table A1.1: MOSFET, BJT and IGBT Characteristics 25
Table A3.1: Truth Table of PMOS Gate Driver 34
Table B1.1: Costs of components for each prototype 44
Table B2.1: Table showing the Power Losses and Running Costs 46
Table C1: Bill of Materials for the prototype 47
Table G1: Technical specifications of the linear compressor model 56

Introduction

This report documents the linear compressor controller design proposed by Electrical & Electronic Design Limited (EED Ltd.). Commissioned by Fisher & Paykel Appliances New Zealand (FPA), the controller design outlined in this report is intended to serve as a prototype in assessing the effectiveness of using a similar controller in FPA fridges.

FPA outlined five key requirements for the proposed design: control flow rate according to demand via communication with the fridge master controller, avoid piston head collisions in the compressor, maximise drive efficiency at low air flow rates, optimise the overall cost of the system, and provide a specification for FPA during the planning stage of the project. Extra opportunities were identified to detect piston head collisions if they occur, and dynamically adjust the system behaviour to compensate for changes in the controller's resonant frequency (Fisher & Paykel Appliances NZ, 2018).

The proposed design mixes digital and analogue components to control the compressor piston. A microcontroller is used to drive the piston to achieve the desired flow rate, alongside interpreting data provided by analogue sensors to ensure that the compressor is behaving in an expected manner. These combine to ensure the reliability of air flow rate that the compressor outputs.

Section 1 of this report outlines the function and design rationale for each subsection of the proposed circuit. Following this, Section 2 gives an overview of the cost associated with the design. Section 3 introduces the relevant considerations when mass-producing an electronic product, and Section 4 outlines analysis and advice regarding the real-world feasibility of the design. Finally, the appendices provide further details and analysis relating to the proposal.

1.0 Design Functionality

1.1 Overview

The overall functional block diagram for the circuit is shown below in Figure 1. It shows how each subsystem relates to the next and shows the outputs/inputs of each function block. For specific implementation details, refer to Appendix A.

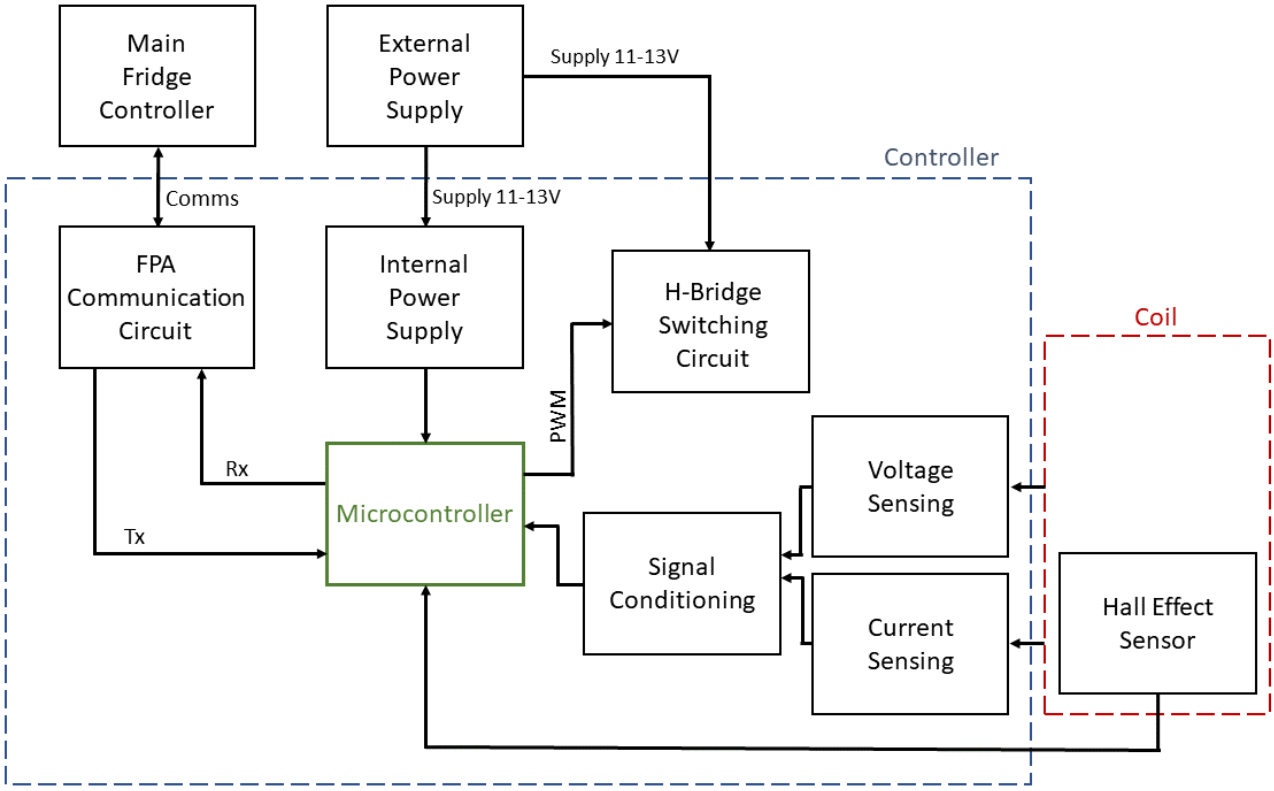

Figure 1: Overall Functional Block Diagram

1.2 Internal Power Supply

The purpose of the internal 5V supply is to power the various integrated circuits used with a stable 5V source. Since these are often sensitive to changes in voltage, a reliable form of voltage regulation was required. Several designs were considered, and an off-the-shelf regulator integrated circuit (IC) was chosen for its high robustness. The transition from the input voltage of 11-13V to the 5V supply is shown in Figure 2 below.

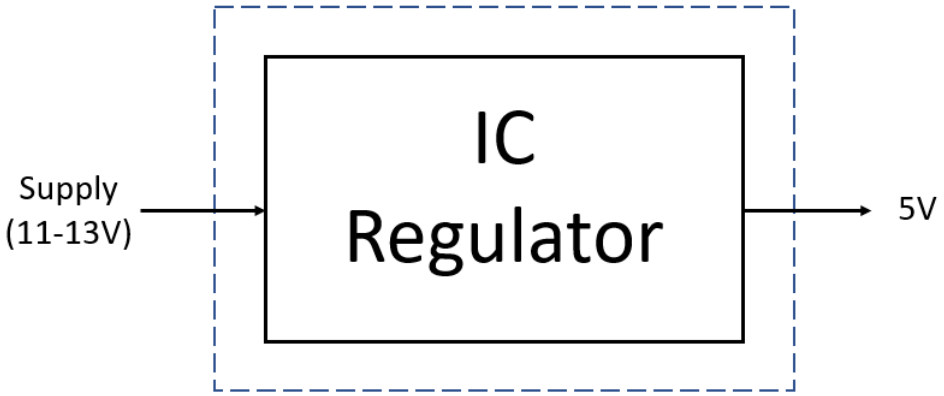

Figure 2: Integrated Circuit 5V Regulator Block Diagram

1.3 H-Bridge

The H-bridge is the circuit used to drive current bidirectionally through the coil and thus produce movement in the shaft.

A major consideration during the design of the H-bridge was how it would facilitate rapid current switching, as this is required to produce specific pumping intensities, while minimising power losses. External drivers were implemented to allow the microcontroller to control the H-bridge, and these were designed to function at high switching rates.
Additions to the H-bridge were made to accommodate the measuring of voltage and current across the coil. These outputs are processed by the voltage and current sensing circuits, then read by the microcontroller. A representation of the H-bridge's functional parts is shown below in Figure 3.

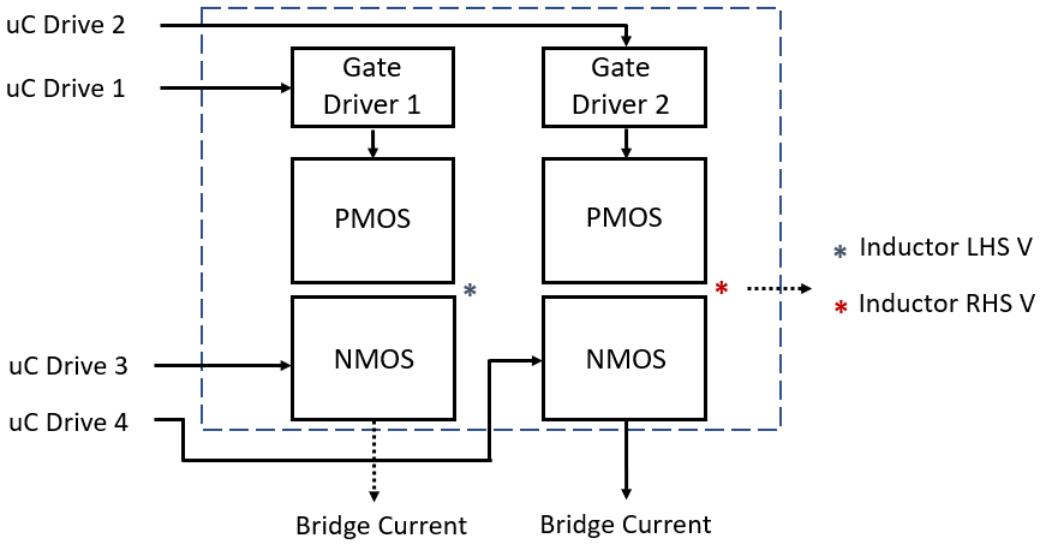

Figure 3: H-Bridge Block Diagram

1.4 Voltage Sensing

The purpose of the voltage sensing circuit is to sample and process the voltage signal across the coil, to obtain voltage and power information for communication with the master controller.

The voltage sensing circuit as shown in Figure 4 processes the Left-hand side (LHS) and Right-hand side (RHS) voltage signals by applying an attenuation to scale the 11-13V across the coil to 0-5V, to utilise the full ADC range. The signal is also level shifted to account for the worst-case scenario while serving as a buffer between the coil and the microcontroller to ensure robustness and reliability.

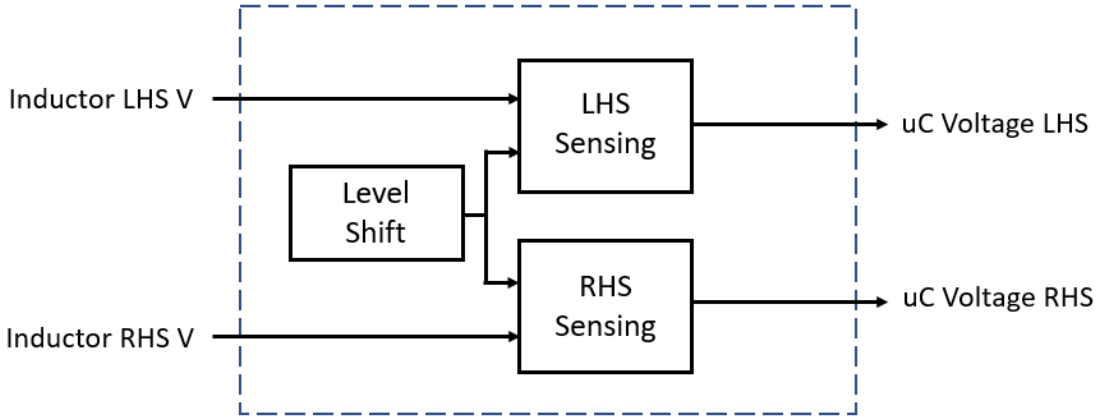

Figure 4: Voltage Sensing Block Diagram

1.5 Current Sensing

This current sensing circuit measures the current through the coil to obtain information about coil blockage, current and power usage for communication with the master controller.

A pair of shunt resistors is used to measure the current flowing through the H-bridge. These have been designed to be small to minimise power loss thus improving efficiency, while having a high-power rating for robustness under high current conditions. The current sensing circuit also contains amplification to utilise the full ADC range, while serving as a buffer between the microcontroller and the coil. The signal is also level-shifted to account for the worst-case scenario to improve robustness. The process from receiving current to providing input to the microcontroller is shown in Figure 5.

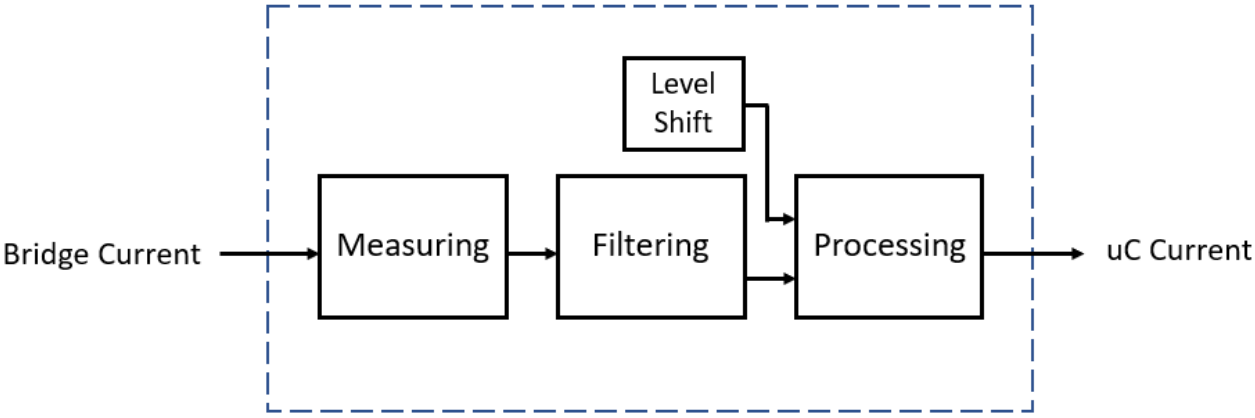

Figure 5: Current Sensing Block Diagram

1.6 Communications Circuit

The communications circuit allows the transfer of information between the compressor controller's microcontroller and the fridge master controller. It uses the FPA ZS5196A communications protocol so that it will function appropriately in a wide range of FPA fridges.

The main aspect of the communication between the master controller and the slave controller relates to the pumping intensity that is required from the linear compressor. The master will provide a number from 0 to 255, with 0 requiring the motor to stop and 255 being the maximum possible pumping intensity. A JSON interface is used for communication. Due to the ambiguous nature of what the number from the fridge master would represent physically, a decision was made to interpret the number received as the stroke length that the linear compressor shaft should use, with 0 relating to no shaft movement and 255 relating to the largest stroke length that the motor can safely operate at. The frequency of shaft movement is maintained at a constant frequency, which has been set at a value close to the system's resonant frequency in order to maximise efficiency. Variations in resonant frequency would ideally be detected by the controller and adapted to in order to further increase efficiency.

The communication circuit's inputs and outputs are outlined in Figure 6 below.

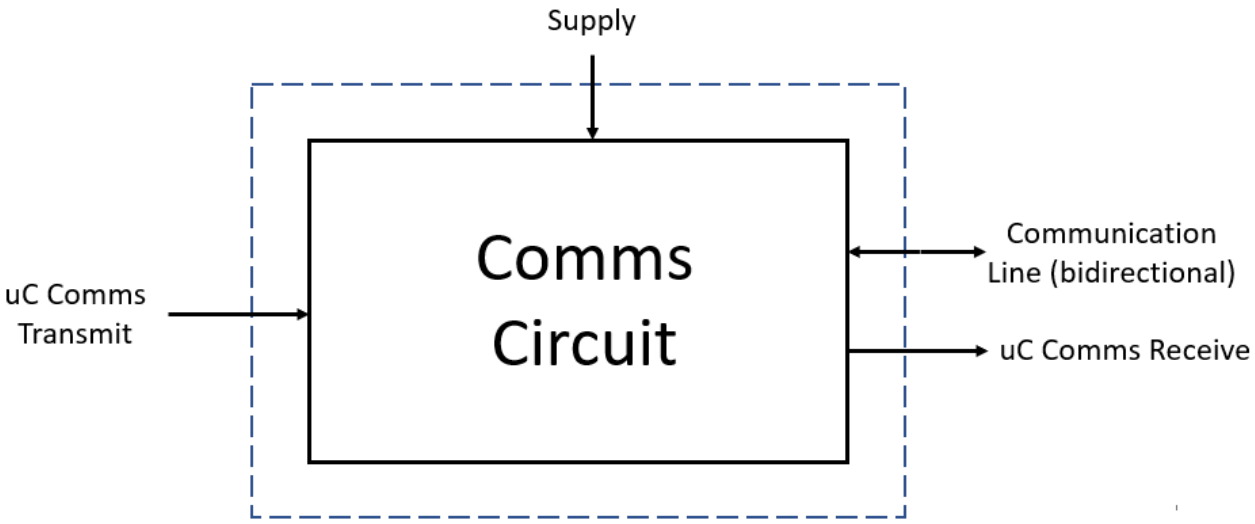

Figure 6: Communication Circuit Block Diagram

2.0 Code Functionality

2.1 Software Architecture Diagram

Figure 7 shown below demonstrates the overall structure of the software that controls the functionality of the motor while communicating with the master controller. Functions and separate files were used to encapsulate objects, separate concerns and offer a level of abstraction to improve readability. High cohesion between the code was applied to decrease interdependence between different sections of code, improving maintainability. The software has 4 main components: the main loop, the UART Receive ISR[1], UART Transmit ISR, PWM ISR.[2]

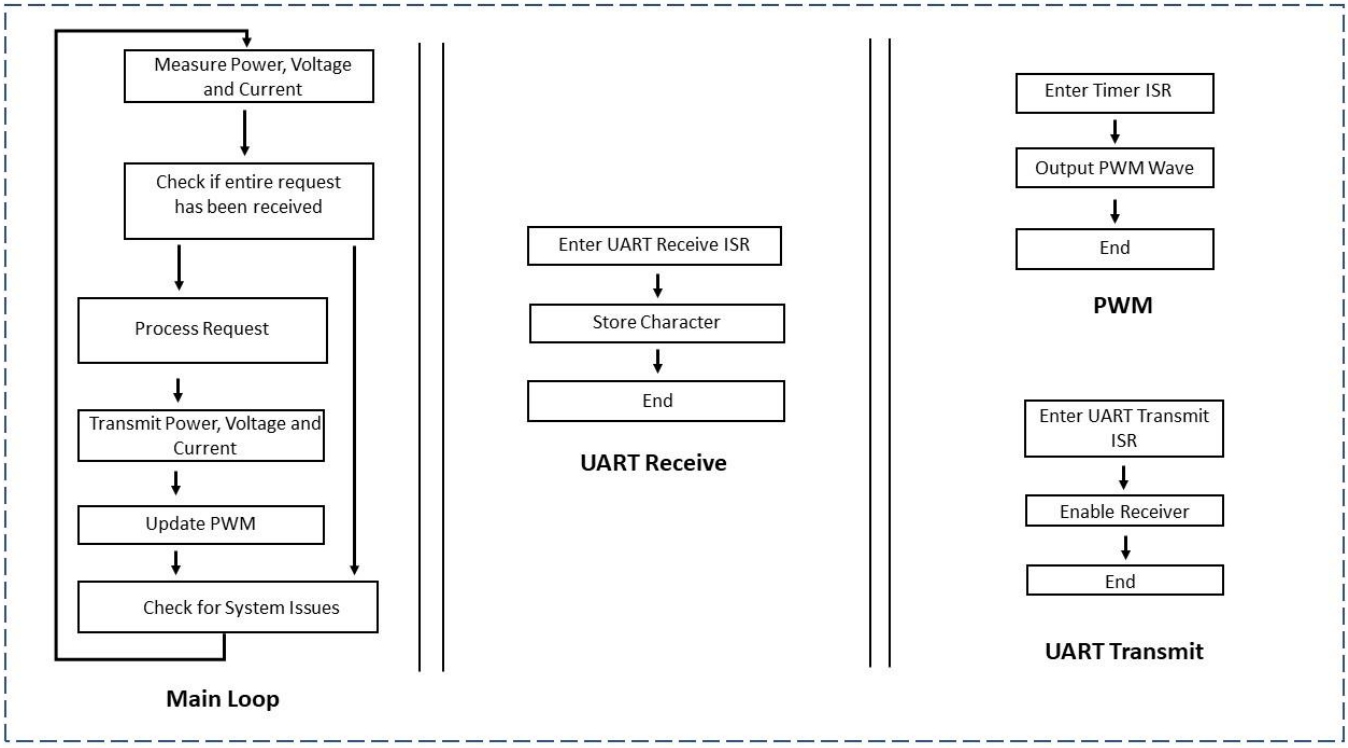

Figure 7: Overall Code Flowchart

[1] ISR – Interrupt Service Routine: Operations that are carried out by pausing current operation – High Priority
[2] PWM: Pulse Width Modulation: Refers to the wave that is operating the motor

2.2 Main Loop

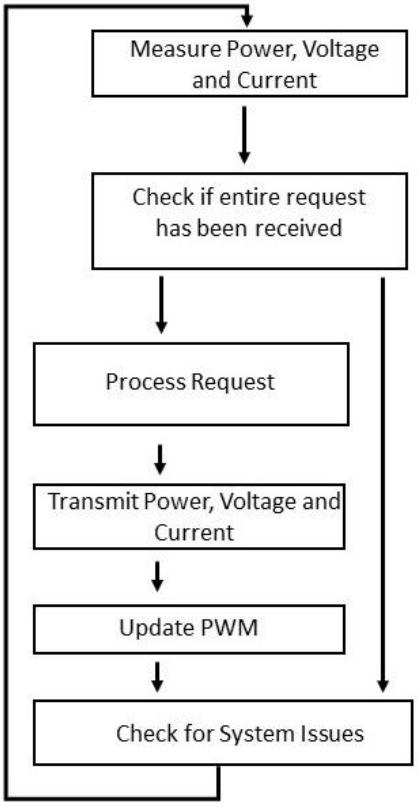

Figure 8: Main Loop Flowchart

The main loop is shown below in Figure 8. The main loop contains functionality to be executed continuously during operation including communication with the master controller and motor control.

The main loop initially reads measurements from the ADC[3] and calculates voltage, current and power before the system responds to a request from the master. This is done so the system is ready to transmit the latest measurements upon request from the master controller. After communication is executed, the system checks for errors. If an error is found, then the motor is shut down until it is resolved.

When information is received, the loop will also update the PWM to reflect any changes in user requests. If operating at a low flow the microcontroller will only pump from one side, in one direction. If the user wishes for zero flow then all microcontroller functionality, except for the transceiver, is shut off to maximise power efficiency.

2.3 UART Receive ISR

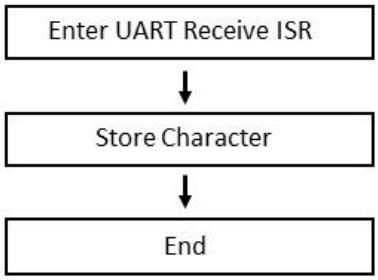

Figure 9: UART Receive Flowchart

Figure 9 shows the functionality of the UART receive ISR. This function's purpose is to create a fast channel of communication between the master controller and the slave controller to relay requests, such as measurement information and motor control. It does this with interrupts to ensure reliably rapid communication.

[3] ADC: Microcontroller peripheral that measures the voltage at an input

2.4 UART Transmit ISR

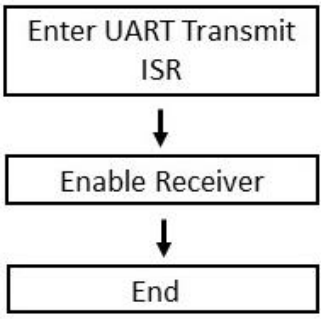

Figure 10: UART Transmit Flowchart

The UART Transmit ISR is shown in Figure 10**.** The purpose of the UART Transmit ISR is to re-enable the receiver after the transmission is complete. The use of interrupts avoids echoing on the half-duplex communication line. The receiver is disabled to ensure it avoids interrupting any transmission, as the FPA circuit has a single bus on which both the receive and transmit signals travel. This ISR enables receive after transmission is complete to return to normal operation.

2.5 Pulse-Width Modulation ISR

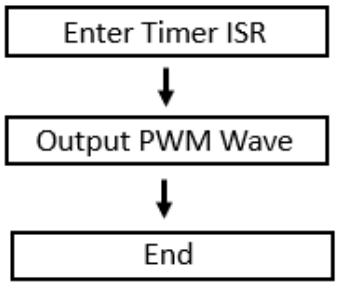

Figure 11: PWM Flowchart

Figure 11 shows the Pulse-Width Modulation ISR. The purpose of this ISR is to produce the waveform that controls the motor's movement. The use of timer interrupts prioritises this operation above all else to ensure the continuous operation of the motor amongst all other functions. The PWM is formed such that it outputs a duty cycle proportional to the requested flow rate, but not high enough such that it causes piston head collisions.

3.0 Cost of Design

The total cost of producing one linear compressor controller is estimated to be close to $7.60 NZD. In accordance with FPA's requirements, the cost has been optimised – it was kept to a minimum while maintaining the quality that end-consumers expect from a premium appliance brand. A more detailed breakdown of cost is shown in Appendix B.
The total cost figure above assumes that Fisher & Paykel Appliances will purchase parts in batches of 10,000 directly from DigiKey NZ. This is based on their intention to manufacture this product in batches of 10,000.

The design was also optimised to reduce energy consumption, reducing customers' energy bills. An explanation of what constitutes the running costs is displayed in Appendix B. The cost savings per year are in the area of $15 NZD/year. This is approximately 10% the annual running cost of a fridge (EECA, n.d.), and emphasises the high-end, energy-efficient nature of FPA fridges. Detailed calculations can be shown in Appendix B2.

4.0 Manufacturing Considerations

There are many considerations to take into account when designing electronics for mass production. The most important of these is the variability of device characteristics that arise due to imperfect manufacturing. For example, each individual integrated circuit has a slightly different current capacity (Guillemin, 2018). The design shown in this report considers the worst-case scenario for each component, so that it will function properly regardless of the variation of components from their normal characteristics. By ensuring that manufacturing variability does not have an effect, this design will minimise faults and returns of the final product. Further details on the most important limitations are shown in Appendix G.

5.0 Testing Overview

The prototype was tested under laboratory conditions, communicating via the prescribed FPA communications protocol and using a wide variety of pumping intensities. An overview of the testing procedure and results are provided in this section.

In order to effectively test the controller, a testing rig was constructed to emulate a linear air compressor using a combination of springs and magnets. This was used throughout the development process and is pictured in Figure 11:

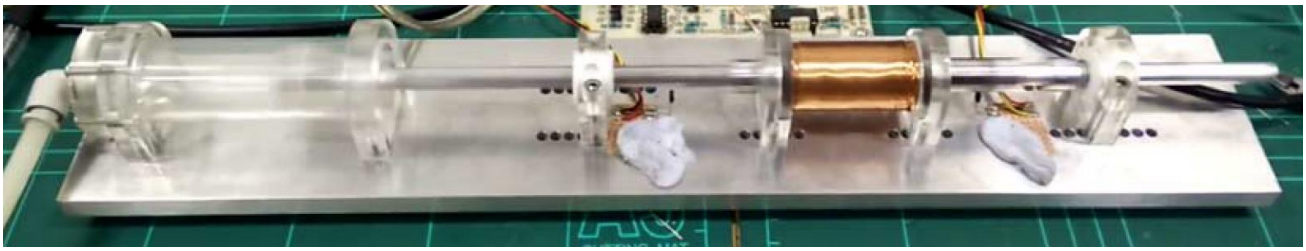

Figure 12: Picture of Linear Motor Rig

The various electronic subsystems within the controller were first tested for correct functionality and the results of this can be found in Appendix D2**.** These tests confirmed that the hardware was performing as designed.

The performance of the design was first tested using regression analysis to determine the relationship between duty cycle and various parameters, such as the voltage across the coil and the current in the coil. The results showed a linear relationship between duty cycle and voltage, and duty cycle and current. More details of this analysis can be found in Appendix D1. The relationship co-efficients were then used to develop mathematical models between MFC requests (the fridge master's desired pumping effort) and the corresponding duty cycle/current output.

Performance was further tested by using a flow-rate gauge, to test the mass flow rate to various MFC requests using the supplied terminal simulating the master controller. The data is summarised in Figure 13 and Table 1 below. The results show that as the magnitude of the MFC requests for pumping effort increases, so does the flow rate. The sudden spike in flow rate between 178 and 179 corresponds the switch from low to high power mode, as requested in the client brief.

Table 1: Table showing the MFC Request vs Flow Rate

50	3
75	3.5
80	6
100	7
150	9
178	10
179	13
254	15
255	16

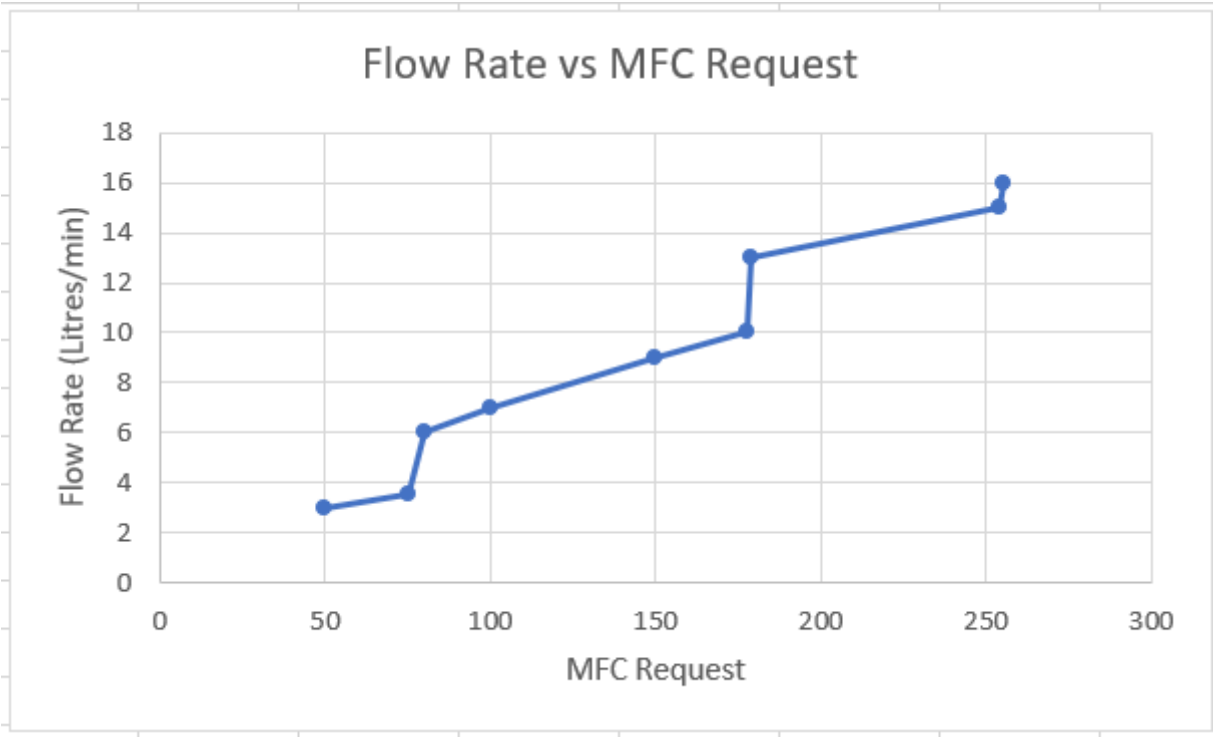

Figure 13: Flow Rate vs MFC Request Graph

As shown, a semi-linear relationship between measured flow rate and requested pumping intensity was produced. A large portion of the variability in the relationship can be attributed to the low accuracy of the flow rate gauge used.

6.0 Design Feasibility

The testing above shows that the design functions as expected in restricted laboratory conditions. However, there are several possible limitations to be considered when assessing the viability of the design in the real world.

Variations between testing rig and real linear motor:

The testing rig was designed as a reasonable approximation to the fridge linear motors. However, there will be variations in parameters between the simulated coil and the actual coil that need to be accounted for. Such differences could include the inductance and resistance of the coil, as well as the mechanical properties of the system. Such variations would require minor modifications in the controller implemented in the fridge. For example, to account for variations in inductance between the simulated and actual coils, the amount of deadtime provided by the PWM wave would need to be changed to make sure there is sufficient time for the coil to discharge.

Effect of Temperature

The controller would also need to be stress tested under various temperatures. The controller was primarily tested under laboratory conditions at approximately room temperature. However, the temperatures experienced by the real controller could vary depending on where it is placed in the fridge, for example placing it close to the condenser could result it in experiencing higher temperatures as opposed to elsewhere in the fridge. However, the components have been chosen to withstand a reasonable range of temperatures, with temperature having the greatest effect on the ATMEGA328P, which operates predictably between -40 to 105^{o}C.

Another effect of varying temperatures on the controller is the amount of dead time[4] needed for the PWM wave driving the pump. An increase in the temperatures will result in the inductance and resistance also fluctuating. For example, at 0^{o}C, the coil resistance (R_{coil}) is expected to be 3.6Ω and inductance (L_{coil}) to be 5.5mH, which results in a discharge time of 9ms. However, at 60^{o}C, R_{coil} is expected to increase to 4.5 Ω and L_{coil} to decrease to 4.5mH, resulting in a discharge time of 6ms. Such variations would mean that dead-time would likely require adjustment to ensure that there is sufficient dead time to avoid errors in operation.

[4] Dead-time: Time in the PWM wave allocated to allow the coil to discharge

7.0 Conclusions

Fisher & Paykel Appliances NZ commissioned this project with the intention to design and test the feasibility of a controller for linear air compressors in fridges. EED has produced a prototype that operates under an 11-13V DC range and demonstrates the viability of the design.

The proposed design meets FPA's key requirements. Flow rate is controllable from the fridge master controller and testing has shown that a semi-linear relationship has been established between the flow rate level requested and the actual flow rate output. Piston head collisions have been avoided by controlling the maximum stroke length at which the pump can operate. Drive efficiency at low flow rates was maximised via driving the coil from one side, along with shutting down all unnecessary modules of the microcontroller during periods where zero flow is requested. The cost of the overall system has been kept to a minimum while maintaining the high level of quality expected from a premium product – the result of this optimisation is a cost of approximately $7.60 NZD per unit manufactured. In addition, a specification containing an overview of the project plan was provided to FPA before physical implementation commenced.

The design of the linear compressor controller proposed in this report operates as intended under laboratory conditions. However, its real-world applicability depends partially on its performance under temperatures more widely varying than those in the lab, and on the testing rig's similarity to the actual FPA linear air compressors. Despite these caveats, the design is likely to be a highly reliable and low-cost addition to FPA fridges.

8.0 References

EECA. (n.d.). *Running Costs calculator – Energywise.* Retrieved from https://tinyurl.com/ybxd2jex

Fisher & Paykel Appliances NZ. (2018). *Linear Compressor Controller Design Brief* [PowerPoint slides]. Retrieved from: https://tinyurl.com/yd4oj92k

Guillemin, G. (2018). *Functionality Design Meeting* [Lecture recording]. Retrieved from https://tinyurl.com/y7kaqwaz

MBIE. (2018). *Sales-based Electricity Costs.* Retrieved from https://tinyurl.com/y8j8fm7c

Appendix A: Implementation Details

Appendix A considers the low-level implementation of the design including selection of components, design equation derivations and circuit analysis procedures.

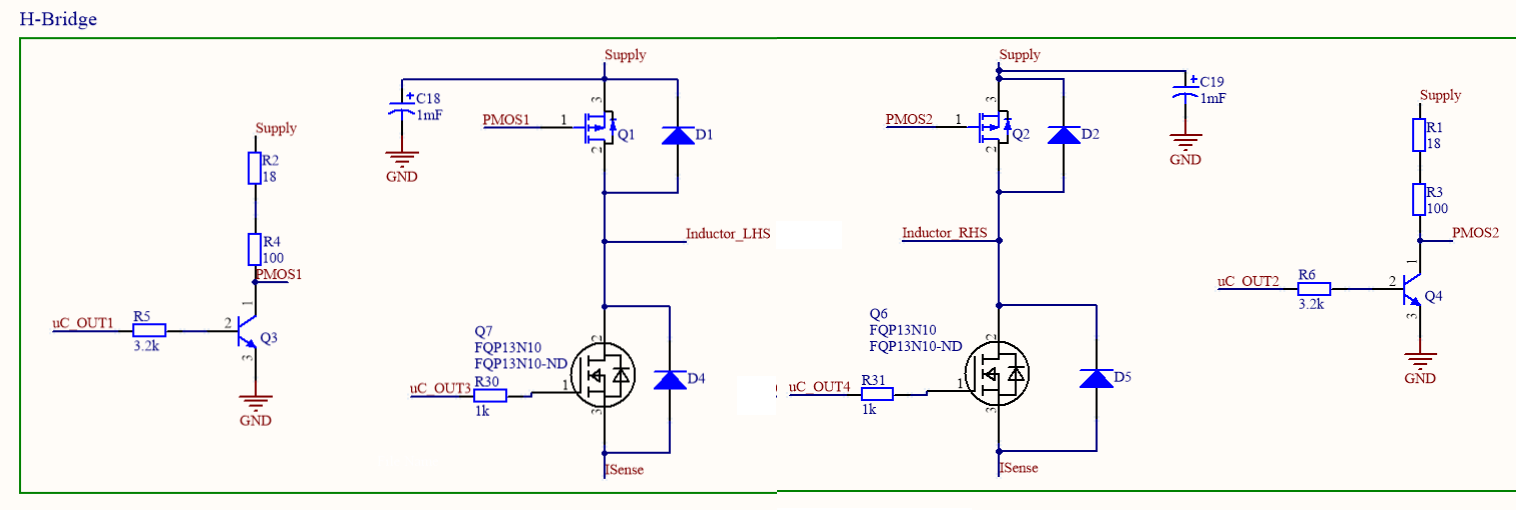

Figure A1: Schematic of the H-bridge

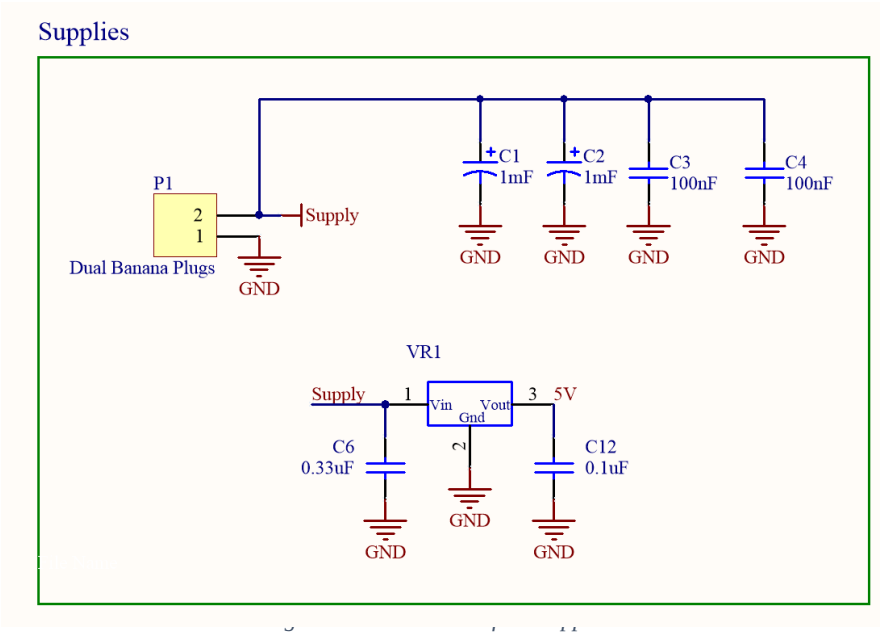

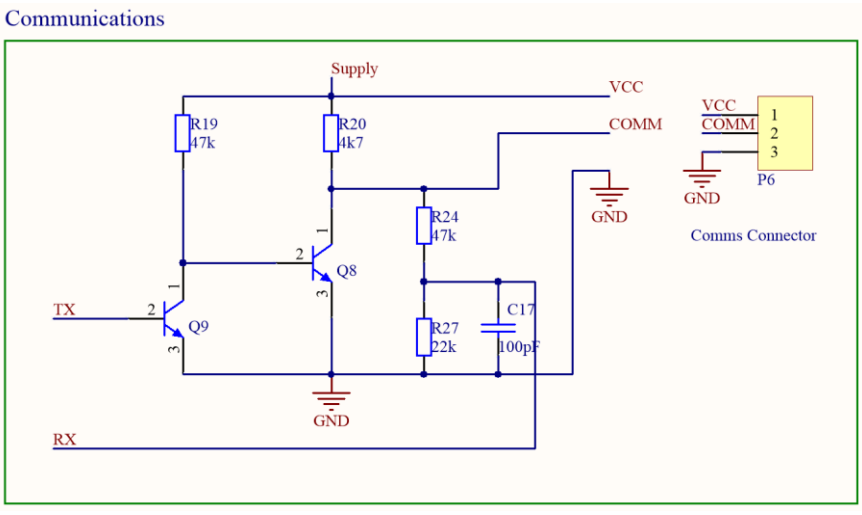

Figure A3: Schematic of the communication circuit

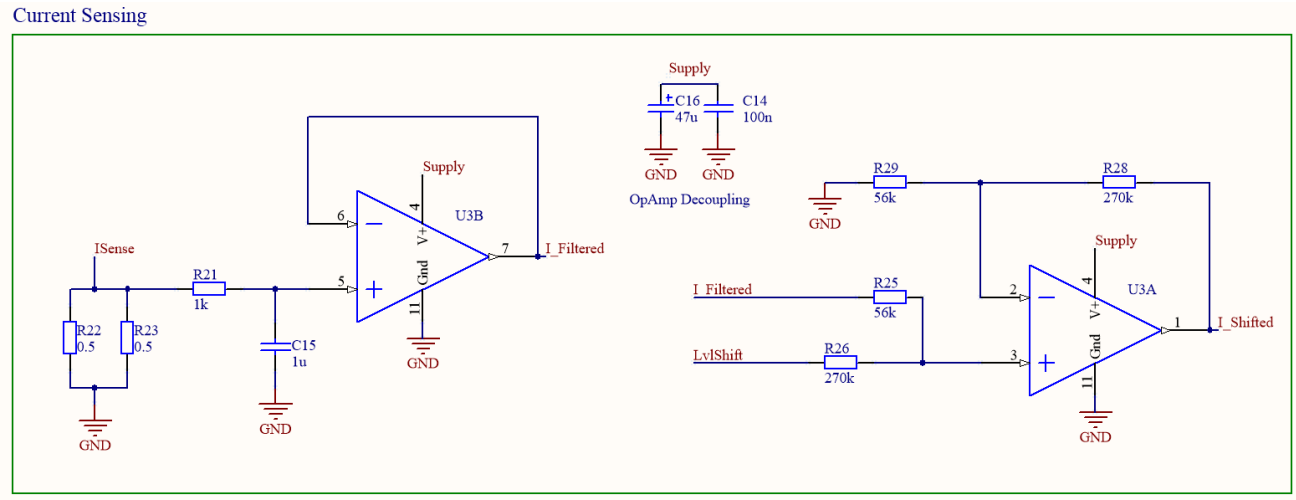

Figure A4: Schematic of the Current Sensing

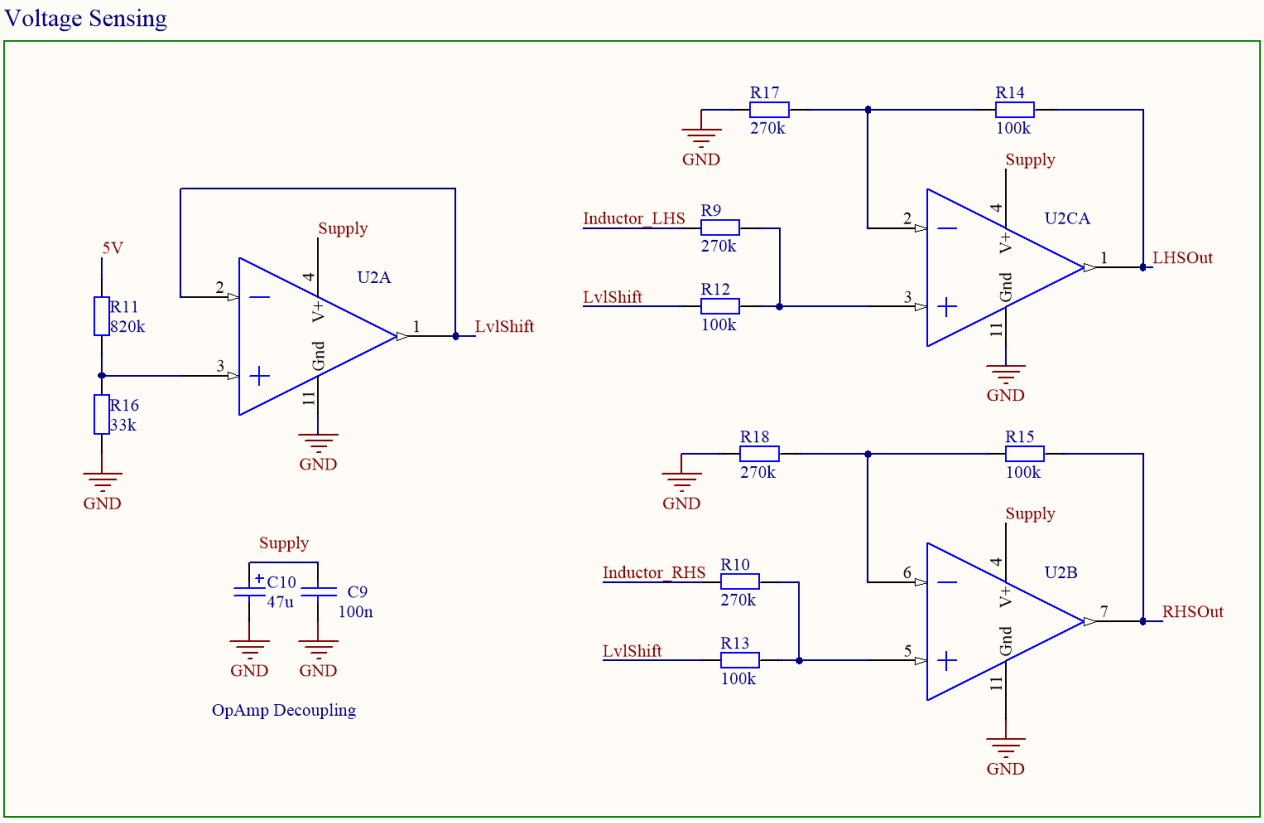

Figure A5: Schematic of Voltage Sensing

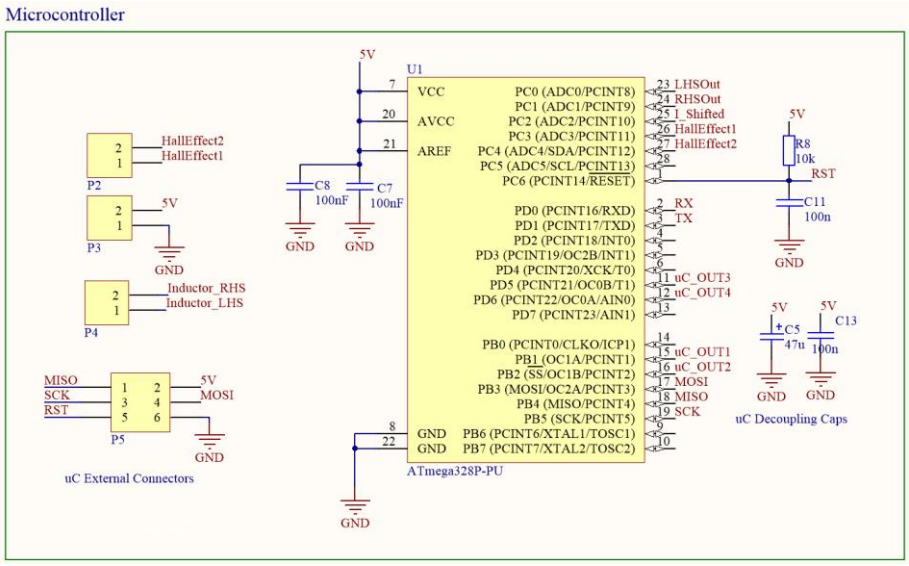

Figure A6: Schematic of the Microcontroller

Appendix A1: Selection of Main Components

This appendix deals with the design rationale used when selecting the main components.

All components were chosen to meet the following requirements, to provide a proof of concept:

Core Requirements:

- Communicate with fridge master controller using the FPA ZS5196A communications protocol
- Control the flow rate applied through the compressor according to demand from the fridge
- Maximise compressor drive efficiency at low air flow rates (<70% maximum mass-flow)
- Optimise the controller system to minimise cost
- Operate between 0°C and 60°C at a voltage of 12V ± 1V DC
- The components were also selected with the goal of detecting shaft jams.

Logic-Level MOSFETs:

To pump the motor back and forth requires control over the direction of current. To implement this, a switching device was required. Devices such as the Logic-Level MOSFETs, Analogue MOSFETs, BJTs and IGBTs were considered. The following crucial characteristics were compared:

Table A1.1: MOSFET, BJT and IGBT Characteristics

Design Factor	MOSFET	BJT	IGBT
Cost	Medium	Low	High
Switching Losses	Medium	High	Low
Switching Speed	Fast	Slow	Medium
Heat Protection	Yes	No	Yes

IGBTs were not considered because of their cost and the lack of need for their high ratings. BJTs weren't considered because of their lack of a heat sink, greater switching losses and slower switching speed. Their greater switching losses are due to the slower switching speeds, which results in a

longer period during which there are high voltage and current transients simultaneously, resulting in larger power losses.

Voltage and current ratings of all three devices were within requirements and therefore weren't considered as a factor.

Finally, Analogue and Logic-Level MOSFETs were considered. The major difference between the Logic-Level and the Analogue MOSFET is the higher switching frequency rating of the Analogue MOSFET. Through testing, it was determined that a high rate of switching (~20kHz) resulted in problems for the MOSFETs regardless of their respective ratings due to the current draw involved. Therefore, considering the lower cost of the Logic-Level MOSFETs, the switching device of choice is the Logic-Level, MOSFET FQP13N10 for low-side switching and the FQP17P10-ND for the high-side switching.

Microcontroller:

The requirement of sensing and adjusting to user requests requires computational power, which requires the use of an embedded device, and thus a microcontroller was implemented. Alternatives to the ATMEGA328P were considered during design. A smaller microcontroller could have been used, as multiple ports on the ATMEGA328P were unused and other microcontrollers also had the characteristics required for this application. One example of a microcontroller that was considered is ATTINY441, which would have reduced the overall cost of the design. The ATMEGA328P was chosen due to its immediate availability and known reliability so that a prototype could be developed. In the final implemented design, smaller microcontrollers should be considered.

5V Regulator:

The microcontroller requires a 5V source to operate. Since it is the most expensive device in the system, careful consideration was taken when choosing its power source.

A simple OPAMP power transistor (with a Zener diode) and a 5V regulator IC were both considered. The advantage of using the OPAMP power transistor regulator is the smaller cost. However, upon experimentation it was concluded that it is less effective in suppressing sudden voltage spikes, which

can reach up to 6V. These can potentially damage the microcontroller and produce irregular ADC readings. To maintain the high reliability that Fisher & Paykel customers expect, the more reliable IC regulator option was chosen.

Current Sensor:

Accurate calculation of current flowing in the coil is important for the estimation of pump power usage.

Different methods of current sensing were considered including: using voltage across the coil and Ohm's Law in combination with known impedance, measuring using shunt power resistors, and measuring using hall-effect sensors.

The original proposal was to use the temperature of the coil to help predict its resistance at any given point in time, thus allowing calculation of the current through the coil. However, the team was informed that the insulating tape around the coil could not be removed. This lowered the feasibility of using a temperature sensor, as only sustained increases in current would produce enough heat to change the insulating tape's temperature significantly, and this lack of responsiveness would lower the robustness of the current measurement system.
The use of Hall Effect sensors to measure current was also not considered due to the complexity of accounting for the impact of the permanent magnets and the movement of the coil on the sensors. Using Hall Effect sensors would also consume extra power as they are active devices.
Hence to measure current, 2 power resistors (placed in parallel with respect to each other) were placed in series with the coil. The combination of a low per-resistor resistance of 0.5Ω and a parallel configuration minimised power dissipation.

Gate Driver Circuit:

The high side MOSFETs cannot be driven directly from the microcontroller and therefore require gate drivers. Gate driver topologies considered include the use of comparator circuits and a BJT switch configuration.

The use of comparators was not a viable option as they require a large pull-up resistor (>1kΩ), for correct operation. Such a pull-up resistor would increase the time constant of the gate driver circuit.

This meant a longer time to charge up the capacitors inside the MOSFETs, decreasing the accuracy of timing for switching.

Therefore, a BJT-driven topology was chosen because of their low cost, and faster response relative to comparators as they can operate with lower value resistors, improving the time constant and thus speed of switching.

Bi-directional Current Circuit:

Several topologies were available to drive bi-directional current through the coil in the manner needed for pumping action to take place.
A centre-tap transformer with a push-pull driver was a theoretically viable driving option, but practical considerations concerning saturation of the transformer and physical configuration of the inductors meant that it was impractical compared to the other options.
Driving using a half-bridge (two switches and two capacitors) was also considered. While this was a simple circuit to implement physically, a major drawback was the limiting of voltage across the coil to half of the supplied voltage due to the voltage divider nature of the capacitor configuration.
The final design uses an H-bridge configuration as it was simple to physically implement and allowed the voltage across the coil to approximately match the source voltage.

Appendix A2: Derivation of Design Equations

This appendix contains the design equations for the proposed linear motor controller outlined in the report. The design equations were derived from the schematics of each of the subsystems.

PMOS Gate Drivers

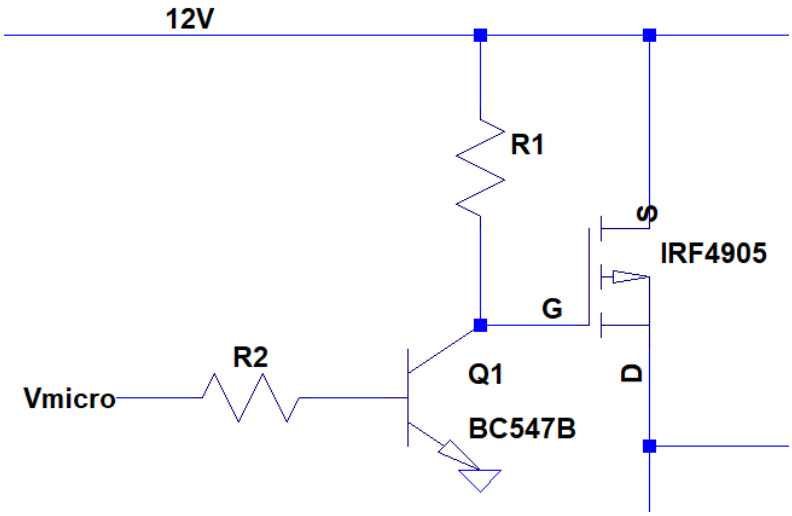

Figure A2.1: Schematic of PMOS Gate Driver

Calculating R_1:

Applying KVL in Figure A2.1:

$$V_{CC} - I_C * R_1 - V_{CE} = 0$$

Since transistor is being driven to saturation, $I_C = I_{CE(SAT)}$ *and* $V_{CE} = V_{CE(SAT)}$

$$V_{CC} - I_{CE(SAT)} * R_1 - V_{CE(SAT)} = 0$$

$$\boldsymbol{R_1 = \frac{V_{CC} - V_{CE(SAT)}}{I_{CE(SAT)}}}$$

Calculating R_2:

Applying KVL:

$$V_{micro} - I_B * R_{B1} - V_{BE} = 0$$

$I_{B(ON)}$:

To ensure that
Since transistor is being driven to saturation, $I_B = I_{B(ON)}$, $V_{BE} = V_{BE(SAT)}$

$$V_{micro} - I_{B(ON)} * R_{B1} - V_{BE(SAT)} = 0$$

$$\boldsymbol{R_2 = \frac{V_{micro} - V_{BE(ON)}}{I_{B(ON)}}}$$

Current Sense - Low Pass Filter

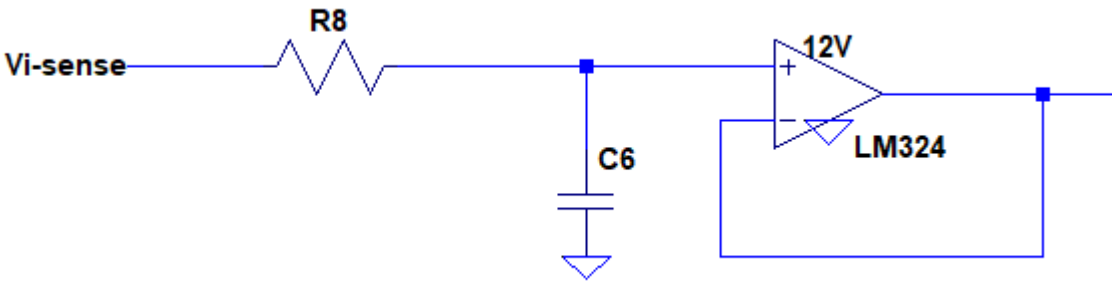

Figure A2.2: Schematic of Current Sense Low Pass Filter

Deriving the transfer function for Figure A2.2:

Since R_{in} of OPAMP = ∞,

Applying voltage divider,

$$V^+ = \frac{C_6}{C_6 + R_8} * V_{i-sense}$$

$$H(s) = \frac{V^+}{V_{i-sense}} = \frac{\frac{1}{sC_6}}{\frac{1}{sC_6} + R_8} * \frac{sC_6}{sC_6}$$

$$H(s) = \frac{1}{1 + sR_8C_6}$$

Calculating corner frequency:

At corner frequency, the gain is -3dB. For this to be true,

$$\lfloor 1 + sR_8C_6 \rfloor = \sqrt{2}$$
$$\lfloor 1 + jw_cR_8C_6 \rfloor = \sqrt{2}$$

Calculating R_8:

$$\omega_c = \frac{1}{R_8C_6}$$
$$f_c = \frac{1}{2\pi * R_8C_6}$$
$$R_8 = \frac{1}{2\pi * f_c * C_6}$$

Level Shifter and Gain Amplifier

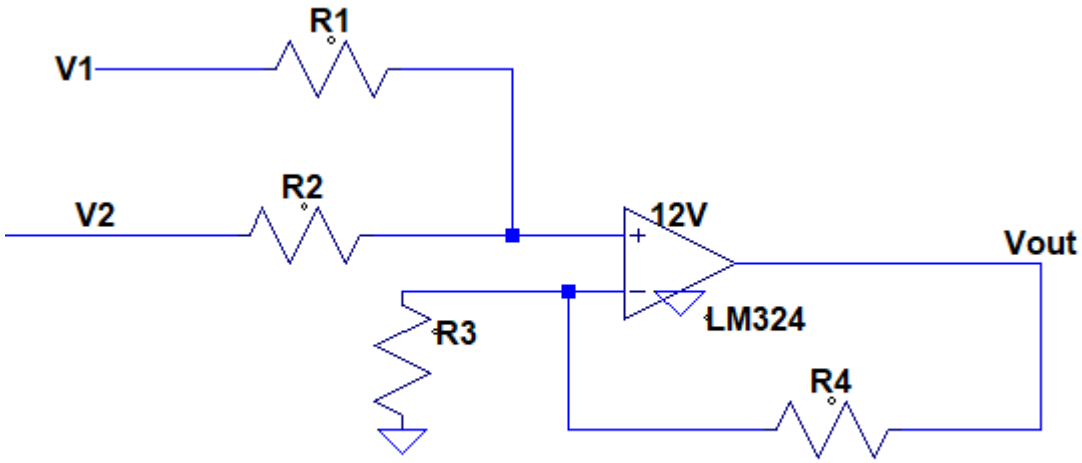

Figure A2.3: Schematic of Level Shifter and Amplifier

Applying the law of superposition to Figure A2.3:

Considering V_1, and V_2 is grounded:

$$V^+ = \frac{R_2}{R_2 + R_1} * V_1$$

Since $V^+ = V^-$,

Applying the voltage divider rule,

:

$$V^- = \frac{R_2}{R_2 + R_1} * V_1 = \frac{R_3}{R_3 + R_4} * V_{out}$$

$$V_{out} = \frac{R_2(R_3 + R_4)}{R_3(R_2 + R_1)} * V_1$$

Considering V_2, and V_1 is grounded:

$$V^+ = \frac{R_1}{R_2 + R_1} * V_2$$

Calculating V_{out}

Since $V^+ = V^-$,

Applying the voltage divider rule,

$$V^- = \frac{R_1}{R_2 + R_1} * V_2 = \frac{R_3}{R_3 + R_4} * V_{out}$$

$$V_{out} = \frac{R_1(R_3 + R_4)}{R_3(R_1 + R_2)} * V_2$$

Adding the voltages as according to the law of superposition,

$$V_{out} = \frac{R_2(R_3 + R_4)}{R_3(R_2 + R_1)} * V_1 + \frac{R_1(R_3 + R_4)}{R_3(R_1 + R_2)} * V_2$$

$$V_{out} = \frac{(R_3 + R_4)}{(R_1 + R_2)} * \left[\frac{R_2}{R_3}V_1 + \frac{R_1}{R_3}V_2\right]$$

Appendix A3: Choosing Component Values

This appendix contains the methods by which component values were chosen.

H-Bridge

The H-bridge configuration works by alternating the direction of the current, which is executed by switching pairs of MOSFETs.

MOSFETs are turned on and off by applying a voltage above and below the gate-threshold voltage ($V_{gs(th)}$), which depend on the type of MOSFET. The high-side MOSFETs were chosen to be PMOS, which have a $V_{gs(th)}$ of -2 to -4V, maximum. The low-side MOSFETs were chosen to be NMOS, which have a $V_{gs(th)}$ of +4.0V, maximum.

The MOSFET states are controlled by the output of the microcontroller, which ranges from 0 to 5V. Hence, the low-side NMOS can be directly driven by the microcontroller's output. However, the high-side PMOS requires gate drivers to produce a $V_{gs(th)}$ of -2 to -4V. This becomes an issue when required to turn off the PMOS, as the 0 to 5V range will not suffice.

Therefore, to drive the PMOS, an inverting power-amplifier BJT transistor switch-circuit is used. This circuit inverts and amplifies the 0 to 5V, PWM signal to 0 to 12V. This results in the desired operation as proven in the truth table below.

Table A3.1: Truth Table of PMOS Gate Driver

PWM – Desired state	**PWM Voltage**	**PMOS – V_g (V)**	**PMOS – V_{gs} (V)**	**PMOS state**
OFF	0 V	12	0	OFF
ON	5V	0	-12	ON

PMOS Gate Drivers

To turn on the PMOS Mosfet (FQP17P10-ND), A $V_{gate\text{-}source}$ of ≈ -4V is required.
This is achieved by using an inverting switch configuration, implemented using a BJT switch configuration.
Referring to Figure A3.1, when the input is high, the transistor is driven to saturation, resulting in V_{cc} being the voltage drop across the collector resistor, resulting in a V_g of ≈ 0 V. Since V_s ≈ 12V, this results in a V_{gs} = -12V.

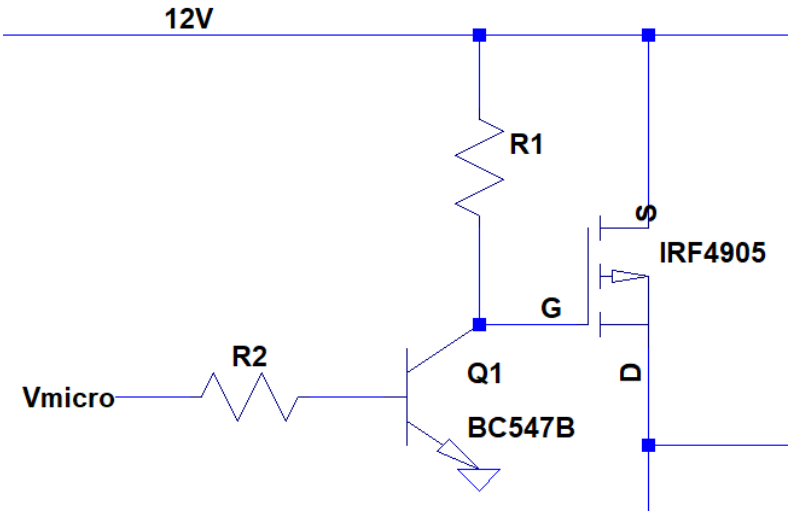

Figure A3.1: PMOS gate driver circuit

Calculating R_c:

$$R_c = \frac{V_{CC} - V_{CE(SAT)}}{I_{CE(SAT)}}$$

Since V_{cc} = 12V, $V_{CE(SAT)}$ = 0.6V, $I_{CE(SAT)}$ = 100mA

$$R_c = \frac{12 - 0.6}{100 * 10^{-3}} = 114\ \Omega$$

Calculating R_b:

$$R_B = \frac{V_{micro} - V_{BE(ON)}}{I_{B(ON)}}$$

Since V_{micro} = 5V, $V_{BE(SAT)}$ = 0.9V, $I_{b(ON)}$ = 5mA

$$R_B = \frac{5 - 0.9}{5 * 10^{-3}} = 820\ \Omega$$

Low Pass Filter

The voltage across the current measurement shunt resistor was observed to have spikes due to the back-emf and was seen to be oscillating as the solenoid charges and discharges. To smoothen the waveform and remove the sudden spikes and thus the high order frequencies, a low pass filter is used.

Many different filters were investigated, including Butterworth, Chebyshev, Inverse Chebyshev, Elliptic and the Bessel filter. A Butterworth type was chosen due to its smooth attenuation in the transition and passbands.

Different orders of Butterworth filters and different attenuated frequencies were considered. A first-order Butterworth was chosen due to a smaller cost (fewer components) and a smaller transient response for reliability.

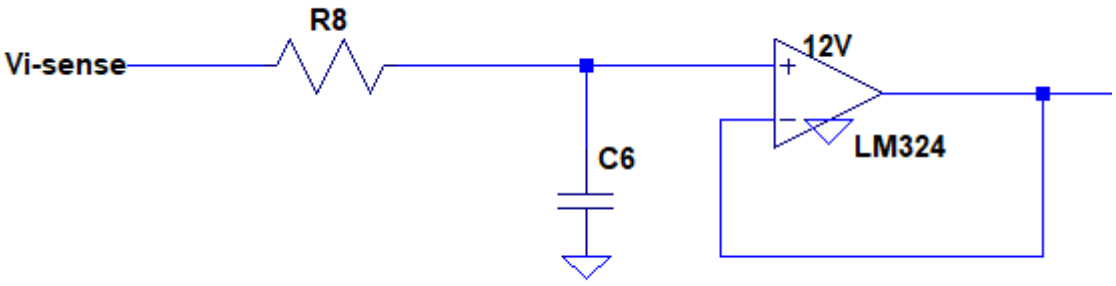

Figure A3.2: Low pass filter circuit

Calculating R_8 and C_6 in Figure A3.2 above

$$R_8 = \frac{1}{2\pi * f_c * C_6}$$

It was observed that at very low corner frequencies, the shape of the waveform was altered, and thus an appropriate corner frequency was determined to be around 150 Hz. This is high enough to remove the high-frequency spikes but also low enough to not disturb the high-amplitude fundamental harmonics that define its shape.

Fixing C_6 = 1 μF, f_c = 150 Hz,

$$R_8 = \frac{1}{2\pi * 5 * 10^{-6}} = 1061\ \Omega$$

Level Shift and Gain Amplifier

To fully utilize and confine to the ADC's range of 0-5V, certain signals are required to be amplified and certain signals to be attenuated. To avoid the scenario of saturation on the lower limits, the voltage is required to be offset by 0.2V. Isolation between the microcontroller and the H-bridge is also required to prevent damage to the microcontroller, which is the most expensive component of the circuit. These requirements are met by using a level-shift and gain amplifier topology as shown in Figure A3.3.

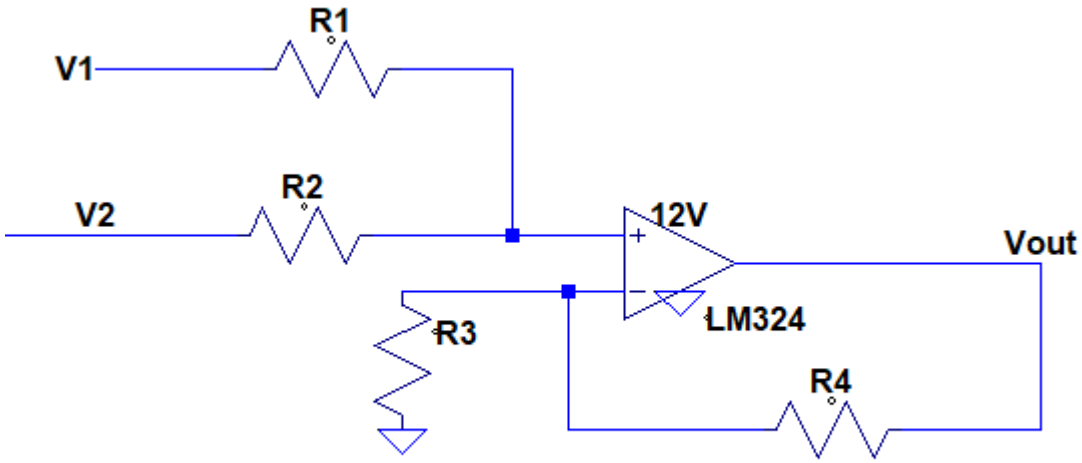

Figure A3.3: Level shift and gain amplifier circuit

$$V_{out} = \frac{(R_{19} + R_{20})}{(R_{17} + R_{18})} * \left[\frac{R_{18}}{R_{19}} V_{measure} + \frac{R_{17}}{R_{19}} V_{shift}\right]$$

Since an overall gain for the sum of the offset voltage and the amplified input is not required, Setting R_{19}=R_{17}, R_{20}=R_{18}

$$V_{out} = 1 * \left[\frac{R_{18}}{R_{19}} V_{coil} + \frac{R_{17}}{R_{19}} V_{shift}\right]$$

Since a gain for the level-shift input in V_{offset} of 0.2V is not required, R_{17}=R_{19}

$$V_{out} = \left[\frac{R_{18}}{R_{19}} V_{coil} + 1 * V_{shift}\right]$$

Voltage Signals – RHS Coil

To measure the voltage across the right-hand side of the coil, the voltage at each end of the coil in a shunt-configuration is sampled. These voltages range from 0 to 13V and thus need to be attenuated to between 0 to 4.8 V (adjusted for offset to avoid the lower OPAMP saturation limit).

An attenuation at worst case scenario is required of:

$$Attenuation = \frac{V_{micro}}{V_{coil-max}} = \frac{4.8}{13} = 0.37$$

Calculating resistor values

Fixing R_{18} = 100kΩ,

$$R_{19} = \frac{100k}{Attenuation} = 270k\Omega$$

Proof of concept:

$$V_{out} = \left[0.37 * V_{coil} + 1 * V_{shift}\right]$$

Since, at worst-case, if $V_{coil\text{-}max}$ = 13V, and since V_{shift} = 0.2V,

$$V_{out} = [0.37 * 13 + 1 * 0.2] = 5V$$

Therefore V_{out} = 5V, which is within the ADC's range.

Final resistor values

Therefore, final values are *R_{17} = 270kΩ, R_{18} = 100kΩ, R_{19} = 270kΩ, R_{20} = 100kΩ,*

Voltage Signals – LHS Coil

Since the requirements for ADC sampling of the left-hand side of the coil is the same as for the right-hand side, the same circuit can be applied to the left-hand side.

Therefore, final values are *R_{13} = 270kΩ, R_{14} = 100kΩ, R_{15} = 270kΩ, R_{16} = 100kΩ.*

Current Signals

To measure the current through the coil, the voltage across the shunt resistor placed in series with the coil is sampled. The maximum voltage expected across the shunt resistor is:

$$V_{max-shunt} = I_{max-coil} * R_{shunt} = 2 * 0.5 = 1V$$

Hence, at worst-case, a voltage across the shunt of 1V is expected. To fully utilise the ADC's range of 0-5V, the signal needs to be amplified to 4.8 V (adjusted for offset to avoid lower OPAMP saturation limit).

$$Gain = \frac{V_{micro}}{V_{shunt-max}} = \frac{4.8}{1} = 4.8$$

Calculating resistor values

Fixing $R_{18} = 100k\Omega$,

$$R_{19} = \frac{270k}{Gain} = \frac{270k}{4.8} = 56k\Omega$$

Proof of concept:

$$V_{out} = \left[4.8 * V_{coil} + 1 * V_{shift}\right]$$

Since, at worst-case, if $V_{coil\text{-}max}$ = 1V, and since V_{shift} = 0.2V,

$$V_{out} = [4.8 * 1 + 1 * 0.2] = 5V$$

Therefore V_{out} = 5V, which is within the ADC's range.

Final resistor values

Therefore, final values are *$R_9 = 56k\Omega$, $R_{10} = 270k\Omega$, $R_{11} = 56k\Omega$, $R_{12} = 270k\Omega$*

Appendix A4: Code Functionality Details

This appendix explains the workings of the code used in the linear compressor controller. The code for each section will be elaborated individually.

Communications:

Communication between the PC and the microcontroller is done through the USART microchip within the microcontroller and the Fisher & Paykel communications circuit that utilises a half-duplex communication bus line.

The half-duplex bus line meant that transmission and receiving would have to be done independently, which was accounted for in the code. Receiving is enabled by default. When a full request is received, the receiver is disabled, so that a response can be transmitted. Upon completion of the transmission, the receiver is then enabled. Since requests could potentially change the operation of the motor, it should be read as soon as possible, and therefore the receiver function is implemented via interrupts.

The USART transmission utilises 1 start bit, 1 stop bit and no parity bits, at a baud-rate of 9600 bits per second.

Flow Rate Control:

Flow-rate control depends on the request by the user, which involves the communication system. The user request which is received through the communication system is then taken and parsed to extract the 3-character request. The three-character request is then converted to a duty cycle using a piecewise linear relationship. This means that the 0-255 request is segmented into different portions to produce a gradual increase in stroke length. The PWM will use this updated duty cycle when it next triggers.

Power Measurement:

Power measurement is done via the ADC readings taken from the voltage sensing circuit. The difference between the sides of the coil is taken to find the voltage across the coil. Current is estimated using Ohm’s Law. The RMS value of the voltage and current are obtained by processing the array through loops. Hundreds of samples are taken across a period to store in an array to obtain

the average values of current and voltage. Power is calculated using the relationship between the voltage across the coil, and the impedance of the coil itself.

The ADC values are read by polling, meaning the code reads values and does not execute other code in the main loop until that reading is complete. ADC reading is sensitive and thus it is essential that code of less importance - specifically power calculations and parameter transmission – does not interrupt the reading and affect the values. This also ensures that the power calculation has a sufficient number of values for high accuracy.

Fault Detection:

Fault detection includes checking for a blocked motor. This involves polling the hall effect sensor, which outputs a voltage proportional to magnetic flux density. Since there are magnets on the pump, this voltage is proportional to the displacement of the pump. If the numbers do not fluctuate as expected, this would imply the motor is not moving. However, this could also be indicative of a low flow request, so the code only reports the abnormal activity if the motor is functioning in high power mode. The motor soft-resets and includes the error in the next transmission. Errors will continue to be included until a request from the master controller specifies that errors should be cleared by attaching the “ew” value to “clr” parameter.

PWM ISR[5]:

A PWM of 1kHz was chosen to be high enough as to provide flexibility with dead-time[6] while being low enough to prevent over-driving the MOSFETs. It was found through experimentation that driving at high frequencies (>5 kHz), results in large voltage ripples which couldn’t be regulated. The PWM is being driven with timer interrupts that trigger whenever the timer reaches a certain value. This ensures that the motor continues to be driven. If the PWM was driven by polling, then the execution of code in the main loop could delay waves. This would upset the pulses, and possibly drive the motor at an unintended frequency.

[5] PWM: Pulse Width Modulation – refers to a modulated wave formed to drive and control the circuits
[6] Dead-time: Time allocated for coil discharge

Appendix B: Costing Particulars

This appendix contains the cost breakdown of the prototype design, with the cost of each part shown. One of the primary instructions given from FPA was to optimise cost – this has been accomplished by choosing an SMT implementation, finding low-cost variants of each component and minimising the total number of components needed. However, it was also recognised that the controller will be used in FPA's premium fridges. This informed the decision to use several higher-cost components This informed the decision to use several higher-cost components that were more effective than their cheaper counterparts, to maximise the reliability of the design and meet end-consumer expectations of quality.that were more effective than their cheaper counterparts, to maximise the reliability of the design and meet end-consumer expectations of quality.

The cost of each component is tabulated below in Table B1.1 on the following page. There are several costing procedures to note:

- The connectors and banana plugs used in the prototype design have not been assigned a cost, as these were primarily present for ease of testing and it is likely that the final installed design would be wired directly from the board to the fridge.
- Although a thru-hole microcontroller was used during testing to ease installation and removal, an identical SMT variant will be used in the actual product. The cost of the SMT variant has been included instead of the thru-hole variant.
- The Hall Effect sensor was not available at the preferred supplier (DigiKey NZ) so its cost was calculated for a scenario where it is sourced from AliExpress.
- The cost of PCB materials and manufacture has been excluded as this will take place internally at FPA with a cost unknown to EED at this time. Since the manufacturing will take place in very large batches, the costs related to PCBs are not likely to have a significant impact on the total figure.

Appendix B1: Materials Cost

This appendix contains the materials cost for the prototype.

Table B1.1: Costs of components for each prototype

Description	Package Type	Size/Capacity	Quantity	Cost Per ($NZD)	Total Cost ($NZD)
Electrolytic Capacitor	Thru-Hole	1mF	4	0.107	0.428
Ceramic Capacitor	SMT 0805	100nF	9	0.00541	0.04869
Ceramic Capacitor	SMT Cap	47uF	3	0.0748	0.2244
Ceramic Capacitor	SMT 0805	330nF	1	0.00631	0.00631
Ceramic Capacitor	SMT 0805	1uF	1	0.00822	0.00822
Ceramic Capacitor	SMT 0805	100pF	1	0.00318	0.00318
Diode (1N4001)	Thru-Hole		4	0.0281	0.1124
Test Pin	Thru-Hole		16	0.01	0.16
Banana Plugs	Thru-Hole		1	0	0
Connector	Thru-Hole	2 Way	3	0	0
Connector	Thru-Hole	3 X 2 Way	1	0	0
Connector	Thru-Hole	3 Way	1	0	0
Resistor	SMT 0805	18Ω	2	0.00194	0.00388
Resistor	SMT 0805	100Ω	2	0.00212	0.00424
Resistor	SMT 0805	3.2kΩ	2	0.0336	0.0672
Resistor	SMT 0805	10kΩ	1	0.00212	0.00212
Resistor	SMT 0805	270kΩ	6	0.00194	0.01164
Resistor	SMT 0805	820kΩ	1	0.00194	0.00194
Resistor	SMT 0805	100kΩ	4	0.00212	0.00848
Resistor	SMT 0805	33kΩ	1	0.00212	0.00212
Resistor	SMT 0805	47kΩ	2	0.00212	0.00424
Resistor	SMT 0805	4k7Ω	1	0.00212	0.00212
Resistor	SMT 0805	1kΩ	3	0.00212	0.00636
Power Resistor	Thru-Hole	0.5Ω	2	0.126	0.252
Resistor	SMT 0805	56kΩ	2	0.00212	0.00424
Resistor	SMT 0805	22kΩ	1	0.00212	0.00212
Microcontroller (ATMega328P)	SMT		1	1.938	1.938
Op-Amp (LM324AMX)	SMT SOIC-8		2	0.1461	0.2922
Voltage Regulator (L7805)	Thru-Hole	5V	1	0.3261	0.3261
P-Type MOSFET (FQP17P10-ND)	Thru-Hole		2	0.94822	1.89644
NPN Transistor (BC547B)	Thru-Hole		4	0.03497	0.13988
N-Type MOSFET (FQP13N10)	Thru-Hole		2	0.78093	1.56186
				TOTAL	**$ 7.59838**

Appendix B2: Running Costs

This appendix contains the calculations and final value for the annual running cost of the controller.

The controller consumes power, and as such has a running cost. As covered in earlier sections, components were selected to both optimise costs and to maximise efficiency at low flow rates, and this has resulted in a running cost saving of **$15/Year.**

Power consumption consists of three main sections: power supplied by the DC source, MOSFET losses, and shunt losses. Some approximations have been made in the course of the calculations, however we have ensured the cost represents a worst-case scenario.

Power supplied by the DC source uses the equation:

$$P = \frac{1}{T}\left(\int_0^T vidt\right)$$

Which is simplified to:

$$P = \frac{1}{T}(VIt_{on})$$

$$P = VDI$$

Where V = DC value of voltage when supplying, D = Duty cycle of current, I = Peak current

MOSFET losses are split into conduction and switching losses, calculated by:

$$P_{switching} = \frac{V_{DS(off)} I_{D(on)} f}{2}\left(t_{s(on)} + t_{s(off)}\right)$$

$$P_{conduction} = D * I_{D(on)}^2 R_{DS(on)}$$

The two shunt resistors have loss represented by:

$$P = 2I^2R$$

The combination of these figures provides the power consumption of the device. The control request number has been estimated to average at 100 for a year since it should only be on high-power mode when the fridge is left open for an unusually long period. We also assume that the fridge is always

operating. The average cost for energy paid by a residential consumer in 2018 is 16.29¢/kWh (MBIE, 2018).

Table B2.1 below displays the values used in calculations.

Table B2.1: Table showing the Power Losses and Running Costs

Average MFC		100				
Corresponding Duty Cycle		43%				
Operating Frequency		13				
Switching Frequency		1000		**Shunt Losses**		2.25
Mosfet Losses				**Power Supplied**		7.74
Switching Losses	PMOS			**Mosfet Losses**		0.37089
Vds(Off)		12	V	**Total Power**		10.36089
Id(On)	Average	1.5	A	**Hours in a Year**		8760
ts(on)		445	ns	**$/kWh**		0.16
ts(off)		310	ns	**Cost/Year**		14.52182
Switching Losses	PMOS	0.006795	W			
				Without Controller		
Switching Losses	NMOS			**Max Duty Cycle**		99%
Vds(Off)		12	V	**Total Power**		20.90709
Id(On)	Average	1.5	A	**Cost/Year**		29.30338
ts(on)		475	ns			
ts(off)		205	ns	**Savings**		14.78155
Switching Losses	NMOS	0.00612	W			
Conduction Loss	PMOS					
Rds(On)		0.18	Ohms			
Conduction Loss	PMOS	0.17415	W			
Conduction Loss	NMOS					
Rds(On)		0.19	Ohms			
Conduction Loss	NMOS	0.183825	W			
MOSFET Losses		0.37089	W			
Shunt Resistor Losses		2.25				

The device has an expected running cost of $14.52 annually. Without a controller, the compressor would be working without communication with the rest of the fridge. This means it would not be able to adjust its duty cycle to requests and would therefore, overestimate the required pumping effort. Table B2.1 displays a calculation of power with a higher duty cycle, which results in an increase of ~$15 annually, representing the savings generated by using this design.

Appendix C: Bill of Materials

This appendix contains a list of components and their designators relating to the full circuit overview shown in Appendix A. These are shown in Table C1:

Table C1: Bill of Materials for the prototype

Description	Size/Capacity	Quantity	Schematic Designator(s)
Electrolytic Capacitor	1mF	4	C1, C2, C18, C19
Ceramic Capacitor	100nF	9	C3, C4, C7, C8, C9, C11, C12, C13, C14
Ceramic Capacitor	47uF	3	C5, C10, C16
Ceramic Capacitor	330nF	1	C6
Ceramic Capacitor	1uF	1	C15
Ceramic Capacitor	100pF	1	C17
Diode (1N4001)		4	D1, D2, D4, D5
Test Pin		16	Not Shown
Banana Plugs		1	P1
Connector	2 Way	3	P2, P3, P4
Connector	3 X 2 Way	1	P5
Connector	3 Way	1	P6
Resistor	18Ω	2	R1, R2
Resistor	100Ω	2	R3, R4
Resistor	3.2kΩ	2	R5, R6
Resistor	10kΩ	1	R8
Resistor	270kΩ	6	R9, R10, R17, R18, R26, R28
Resistor	820kΩ	1	R11
Resistor	100kΩ	4	R12, R13, R14, R15
Resistor	33kΩ	1	R16
Resistor	47kΩ	2	R19, R24
Resistor	4k7Ω	1	R20
Resistor	1kΩ	3	R21, R30, R31
Power Resistor	0.5Ω	2	R22, R23
Resistor	56kΩ	2	R25, R29
Resistor	22kΩ	1	R27
Microcontroller (ATMega328P)		1	U1
Op-Amp (LM324AMX)		2	U2A, U2B, U2C, U3A, U3B
Voltage Regulator (L7805)	5V	1	VR1
P-Type MOSFET (FQP17P10-ND)		2	Q1, Q2
NPN Transistor (BC547B)		4	Q3, Q4, Q8, Q9
N-Type MOSFET (FQP13N10)		2	Q6, Q7

Appendix D: Testing

Appendix D contains information about the testing procedures undertaken and the results obtained.

Appendix D1: Regression Analysis

Regression Analysis was conducted to determine the relationship between the duty cycle applied and the voltage and current observed in the coil. Graphical results are displayed below with the most relevant relationships coloured.

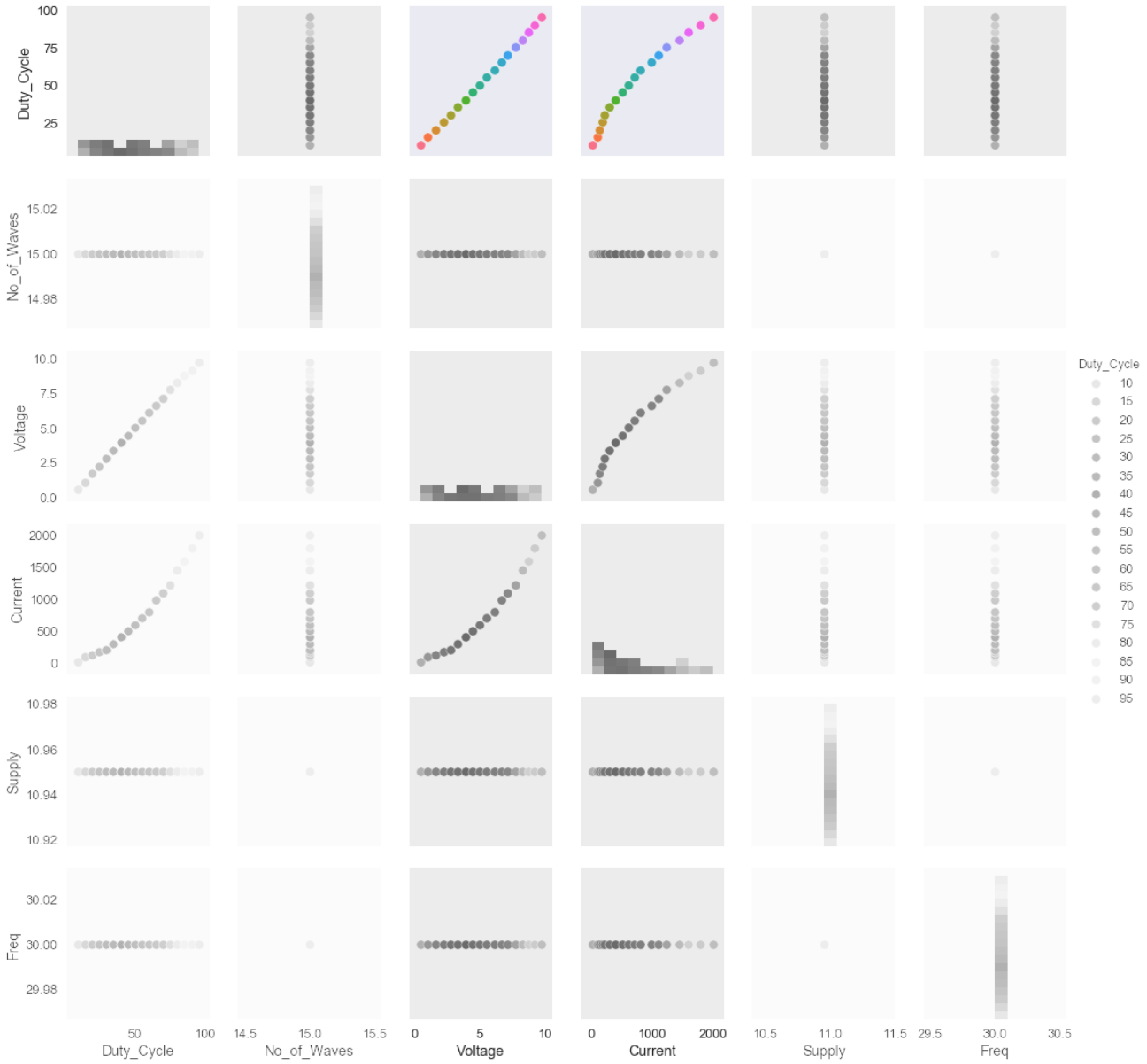

Figure D1.1: Relationships between different variables

Appendix D2: Hardware Testing Results

This appendix contains the waveform results from hardware tests performed.

Hardware functionality was tested by observing waveforms and comparing them to the expected results, as detailed in the waveforms below.

NMOS Gate Voltage

The voltage at the NMOS voltage is ON during the entire corresponding PMOS period to allow the current to discharge safely. During the alternate pair's switching, the corresponding NMOS is switched off. This corresponds to the waveform shown in Figure D2.1.

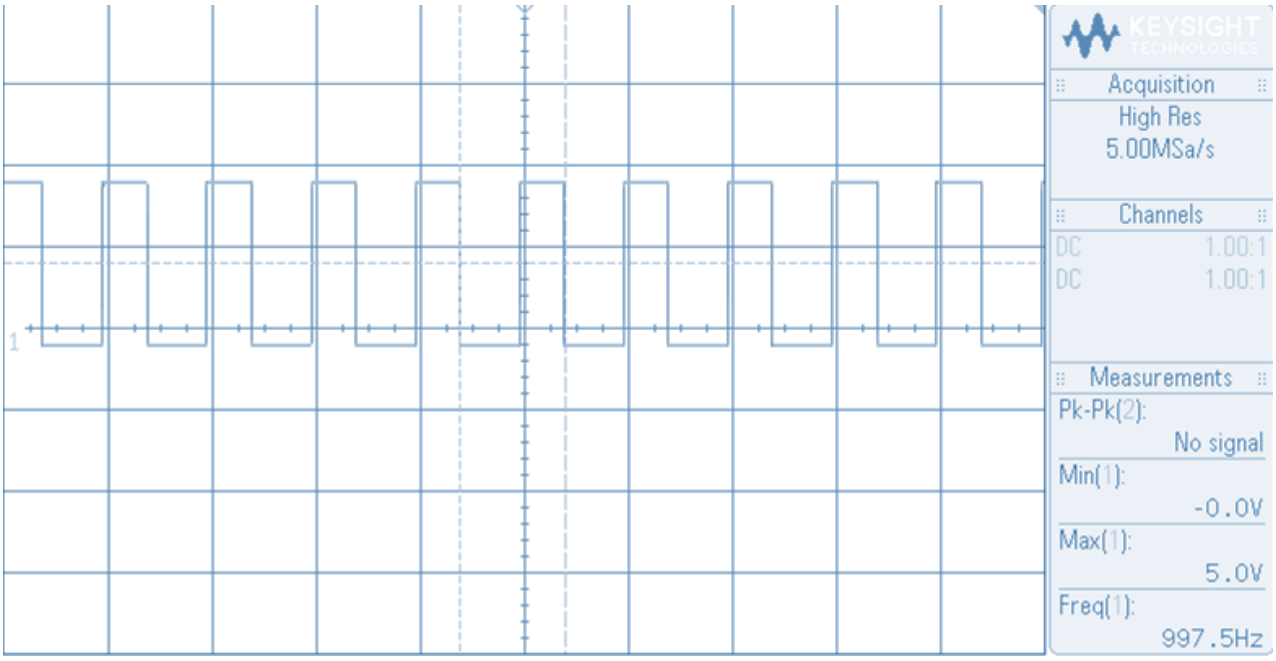

Figure D2.1: Waveform of NMOS Gate Voltage

PMOS Gate Driver Input

The PMOS is being driven according to the PWM output and its ON time corresponds to the duty cycle adjustments. As shown in Figure D2.2**,** there is a periodic signal where there is a section of PWM and a section of OFF time that corresponds to the dead-time.

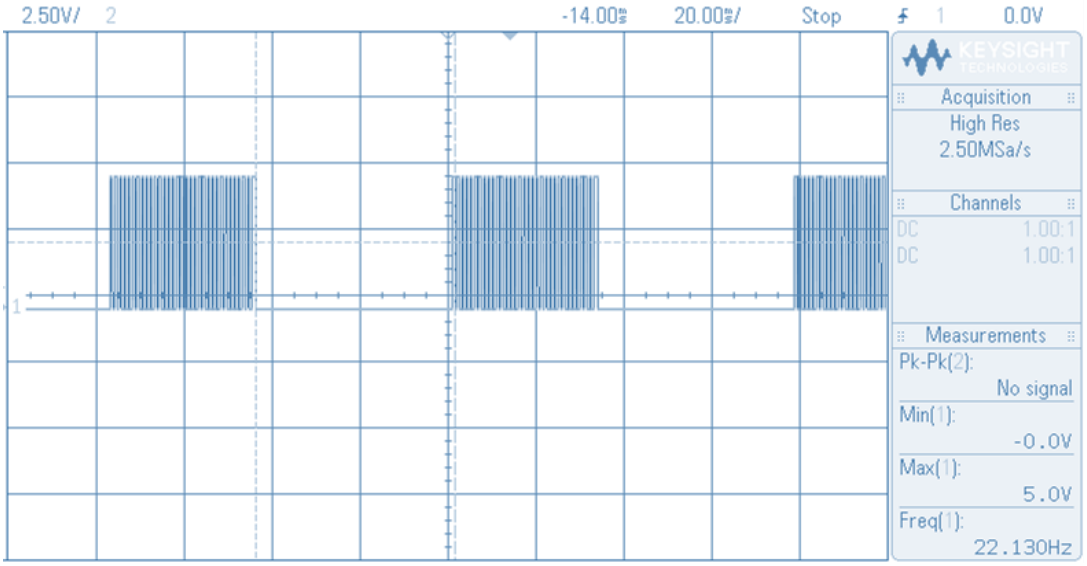

Figure D2.2: Waveform of PMOS Gate Driver Input

PMOS Gate Voltage

The PMOS gate voltage is the output of the inverted amplifier, which therefore should be the inverting and amplified form of the previous waveform, which is what is observed in Figure D2.3 below.

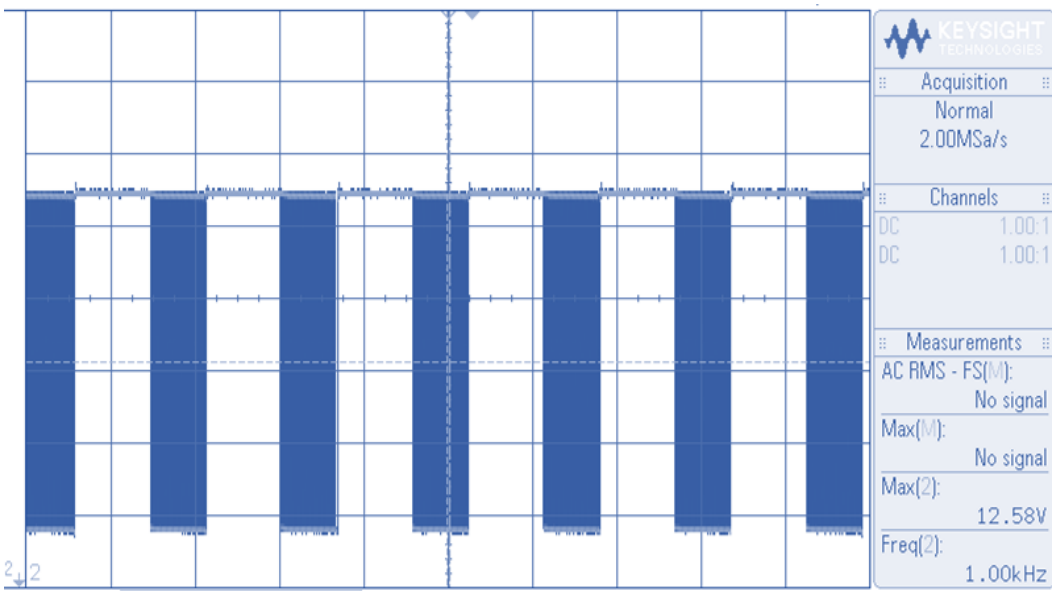

Figure D2.3: Waveform of PMOS Gate Voltage

Current Sense Voltage

The voltage across the current sense resistor should correspond to the current through the coil, and hence there should be a gradual charging and periodic waveform that oscillates according to the PWM that is driving the coil. This is what is observed in Figure D2.4 below.

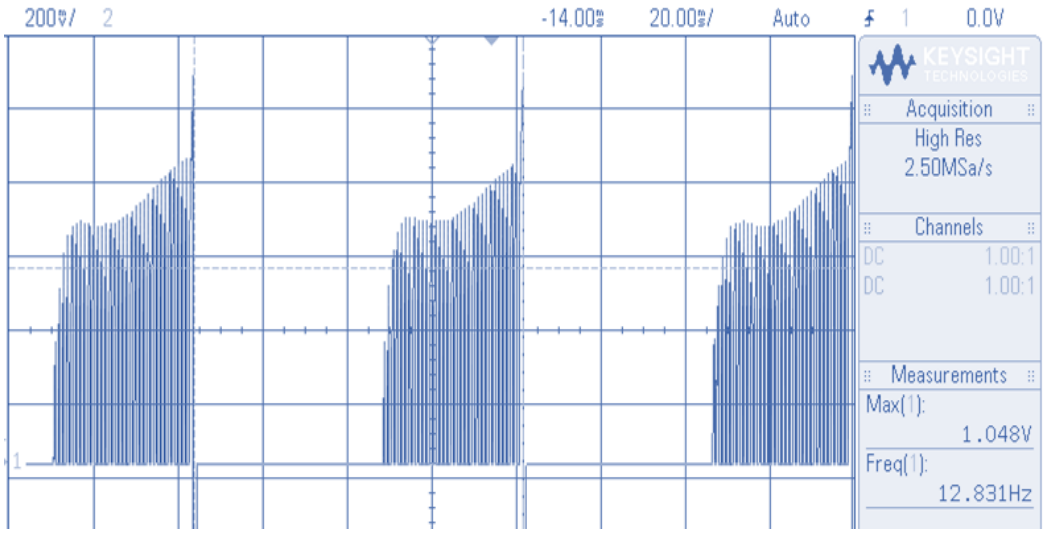

Figure D2.4: Waveform of Current Sense

High-side voltage (Driving with one pair)

When driving with one pair of MOSFETs (low power mode), the voltage across the waveform of the high side should correspond to the PWM driving it. This is what is observed below in Figure D2.5**.**

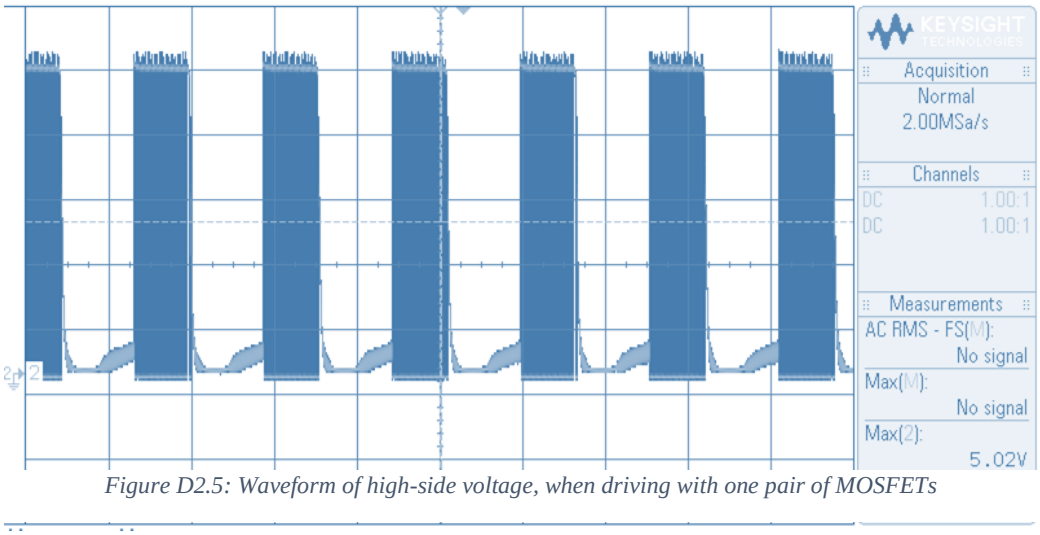

Figure D2.5: Waveform of high-side voltage, when driving with one pair of MOSFETs

Low-side voltage (Driving with one pair)

When driving from one side (low power mode), the voltage at the low side should be the result of the voltage dissipated across the coil, which is what is observed in Figure D2.6 below.

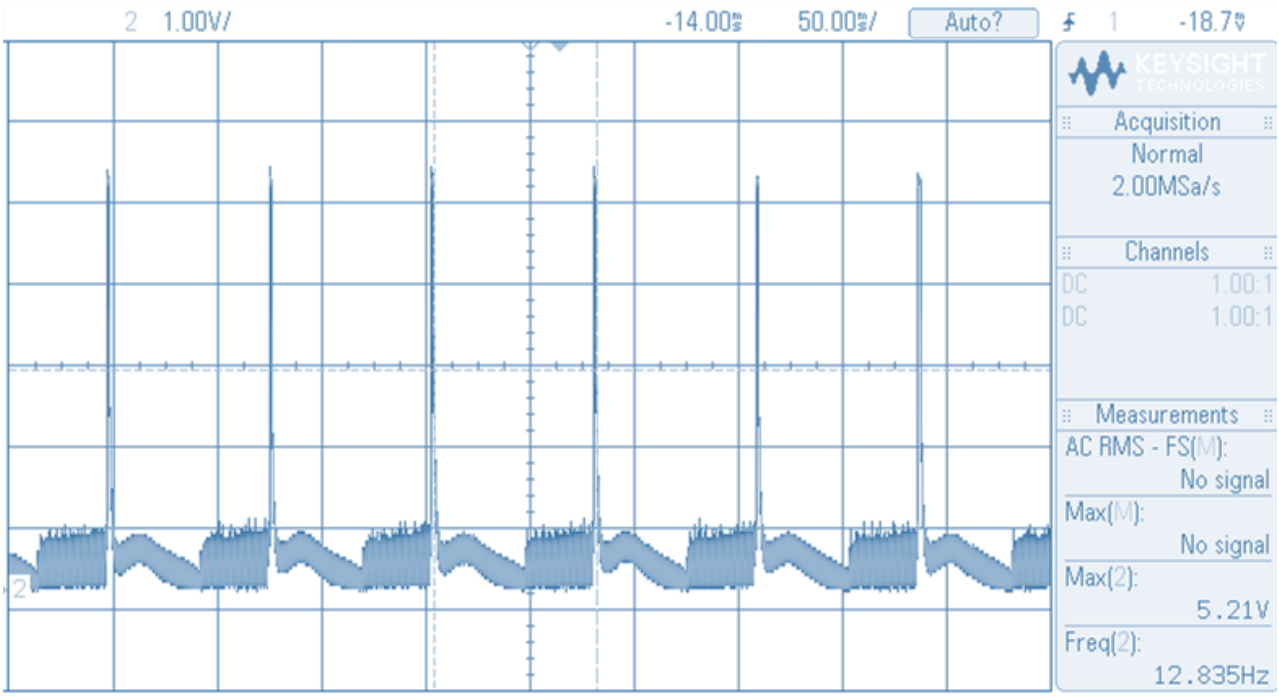

Figure D2.6: Waveform of low-side voltage, when driving with one pair of MOSFETs

Overall, all the waveforms matched their expected shapes. This result, in combination with the successful testing outlined in Section 5.0, indicates that the linear compressor controller functions as expected.

Appendix E: Developmental Process

The details of the process taken to develop the prototype are detailed in this appendix.

For the circuit design discussed in Section 1, different forms of implementation were reviewed. As the goal was to show the viability of the design, development of the design was focused on functionality. Effort was also taken to produce a Printed Circuit Board (PCB) as that is the commercial expectation for electronic systems.

The first step in the development process was the selection of designs, detailed in Section 1. These designs had to be simulated before they were built. The program LTSpice was used to construct circuits and test the subsystems under a range of conditions. Software simulations operate under ideal conditions, so physical methods of testing were required.
Code was set up to drive the H-bridge configuration, allowing the system to be tested with the model motor. In terms of hardware, a breadboard was made to test different sections. Multiple adjustments were required, most of them as a result of components not providing ideal values. After all individual circuits were confirmed as functional, the subsystfems were joined to test the whole system, and the design was found to be functional. Figure E1 below shows a breadboard during development.

After the breadboard was completed, a decision was made to continue to other forms of implementation. This was because the breadboard brings with it many intrinsic side-effects - the numerous wires required introduce parasitic effects, while the connections within the breadboard also interfered with the design (providing additional resistance). Additional capacitors were required at multiple locations on the original breadboard such as the power supply or around ICs. This would not be appropriate for a final design and would also not accurately provide a Bill of Materials, hence the costing and feasibility discussions would not be reliable. With this in mind, a PCB was designed and ordered for the implementation of the final prototype design. The top layer of the PCB is shown below in Figure E2.

After the PCB was completed, effort was concentrated on completing the code. Firstly, a relationship between the duty cycle and the voltage across the coil was required, which was derived through regression analysis. This allowed the user request to be related to the pumping effort of the coil. The next coding step was developing a system to receive the user request through UART. This proved to be a challenge because of the presence of a half-duplex communication line, which prevented

simultaneously transmitting and receiving. The next coding step was to set up the ADC to read the required parameters of voltage, current and power. Different algorithms were experimented to process the voltage values before an approach was decided.

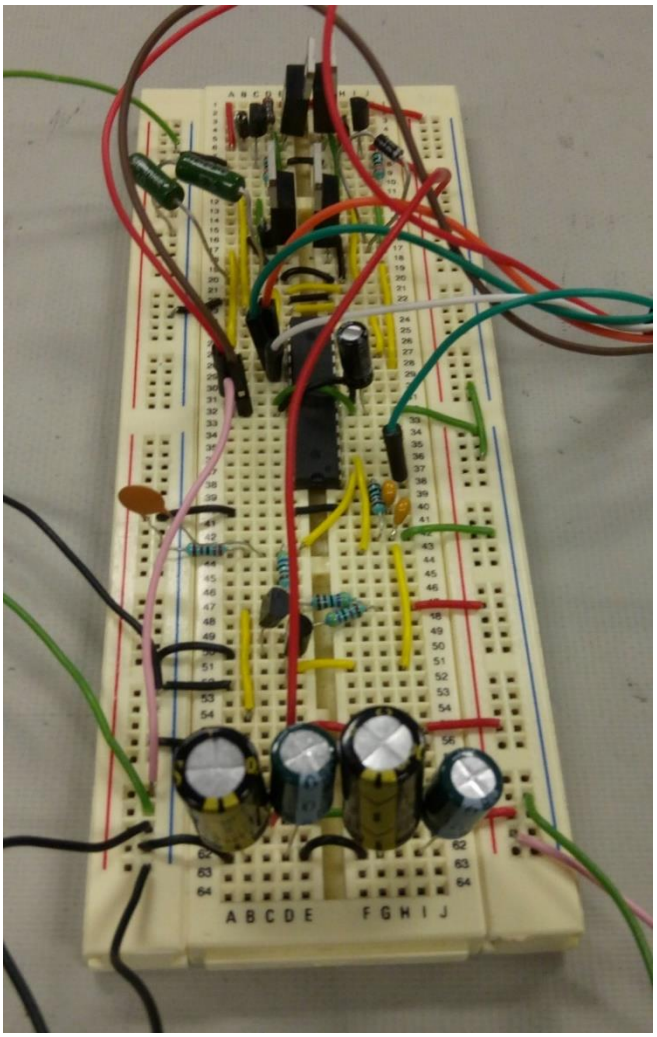

Figure E1: Breadboard during development

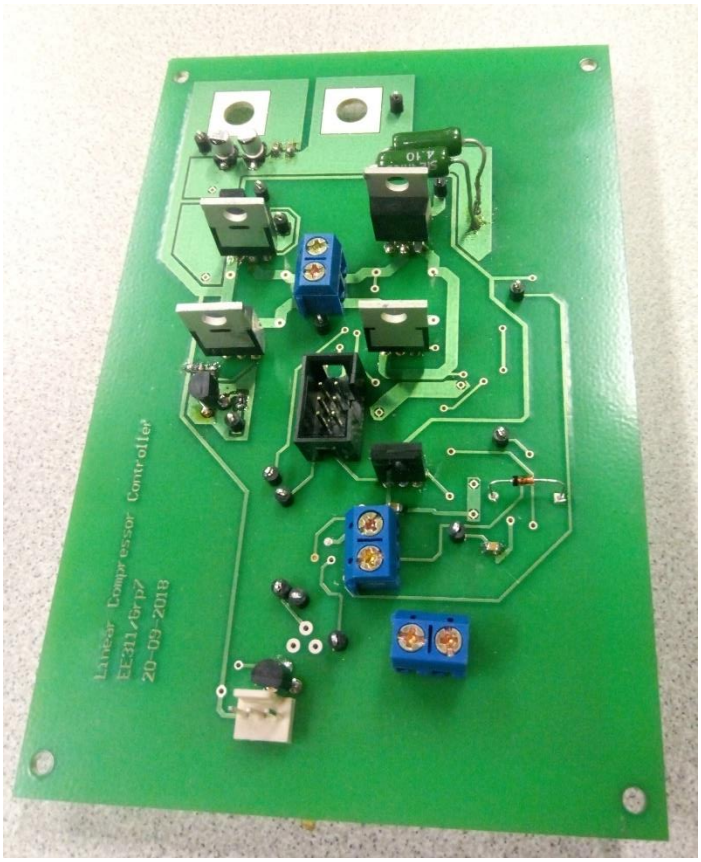

Figure E2: Implementation on a PCB

Appendix F: Manufacturing Considerations

This appendix outlines the considerations taken for the mass-manufactured nature of the products that the controller would be used in.

Due to the variability in device characteristics, the design considered the worst-case scenario for each component. The information required to find each component's worst-case scenario was found in its datasheet. The most significant of these are listed below:

- The resistors and capacitors used in the circuit have tolerances that were considered during the design phase. However, due to the nature of the circuit designed, these had minimal effect on performance, so no measures needed to be taken.

- The LM324 used had varying characteristics in several areas. The most relevant of these was the worst-case output voltage in the range of 0.1-5V when 0V and 5V rails are supplied. Calculations were performed with knowledge of these conditions such as to avoid the lower voltage rail of the 0V by offsetting the input by 0.2V.

- To ensure the high side MOSFETs were switched on completely, the gate driver circuits were designed to drive a gate voltage of exactly 12V when turned on, which would allow for a high amount of drain current to flow. To implement this, the transistor gate driver circuit's collector resistors were designed to ensure that the microcontroller's output would drive the transistor to complete saturation.

Appendix G: Technical Specifications

This appendix provides the technical details for the model that was used to simulate the fridge linear compressor. Table G1 below is separated into the major components of the rig.

Table G1: Technical specifications of the linear compressor model

Component	Value	Notes
Coil		
DC Resistance	4.2 Ω	At 25°C
Resonant Frequency	10.72 Hz	At no-load, 20 degrees
Inductance	5.08 mH	At resonant frequency
Turns	800	
Maximum Current	3.73A	Pump blocked and 0°C
Voltages / Vcc levels		
Supply	12V ± 1V	
Operational Amplifiers	12V ± 1V	Supplied by main supply
Microcontroller	5V	
Hall Sensor Output	0.0675-4.325V	
Permanent Magnet		
Magnetic Remanence	1.28T	
Coercivity H_c	923 kA/m	
Relative Permeability μ_r	1.05	
Spring		
Spring Rate	0.3258N/mm	
Natural Frequency	216 Hz	